Aus der Klinik für Psychiatrie und Psychotherapie
(Prof. Dr. med. J. Wiltfang)
der Medizinischen Fakultät der Universität Göttingen

The role of Neuroligin-2 in fear circuits

INAUGURAL-DISSERTATION

zur Erlangung des Doktorgrades
der Medizinischen Fakultät der
Georg-August-Universität zu Göttingen

vorgelegt von

Lena Marth

aus

Kassel

Göttingen 2022

Dekan: Prof. Dr. med. W. Brück

Betreuungsausschuss

Betreuer/in: Prof. D. Krueger-Burg, Ph.D

Ko-Betreuer/in: Prof. Dr. rer. nat. T. Bayer

Prüfungskommission

Referent/in: Prof. D. Krueger-Burg, Ph.D

Ko-Referent/in: Prof. Dr. rer. nat. T. Bayer

Drittreferent/in: Prof. Dr. R. Dressel

Datum der mündlichen Prüfung: 07.02.2023

Hiermit erkläre ich, die Dissertation mit dem Titel "The role of Neuroligin-2 in fear circuits" eigenständig angefertigt und keine anderen als die von mir angegebenen Quellen und Hilfsmittel verwendet zu haben.

Göttingen, den 30.05.2022 ……

(Unterschrift)

Table of contents

List of figures

List of tables

List of abbreviations

AuC	auditory cortex
AuD	secondary auditory cortex, dorsal part
AuV	secondary auditory cortex, ventral part
Au1	primary auditory cortex
ASD	autism spectrum disorder
BA	basal amygdala
BLA	basolateral amygdala
BSA	bovine serum albumin
CaMKII	calcium/calmodulin-dependent protein kinase II
CA1	cornu ammonis 1
CCK	cholecystokinin
CeA	central amygdala
CeL	centrolateral amygdala
CeM	centromedial amygdala
cNlgn2 KO	conditional Neuroligin-2 knockout
CS	conditioned stimulus
DAPI	4',6-diamidino-2-phenylindole
ddH_2O	double-distilled water
EGFP	enhanced green fluorescent protein
FC	fear conditioning
GABA	γ–aminobutyric acid
$GABA_AR$	γ–aminobutyric acid receptor
GFP	green fluorescent protein
IgSF9b	immunoglobulin superfamily member 9b
IEG	immediate early gene
IL	infralimbic cortex
IRES	Internal Ribosome Entry Site
KI	knock-in
KO	knockout
LA	lateral amygdala
MDGA 1/2	membrane-associated mucin domain-containing glycophosphatidylinositol anchor 1 and 2
mPFC	medial prefrontal cortex
NGS	normal goat serum
Nlgn2	Neuroligin-2
Nrxn	neurexin
NR	nucleus reuniens
OF	open field test
PAG	periaqueductal grey
PB	phosphate buffer

PBS	phosphate-buffered saline
PFA	paraformaldehyde
PTSD	post-traumatic stress disorder
PKC-δ	protein kinase type C
PrL	prelimbic cortex
PV	parvalbumin
S-SCAM	scaffolding protein synaptic scaffolding molecule
SOM	somatostatin
Tac2	tachykinin 2
US	unconditioned stimulus
vlPAG	ventrolateral periaqueductal grey
VIP	vasoactive intestinal peptide
WT	wild type

1 Introduction

As information flows throughout the neural networks of the brain, it is substantially shaped by a highly interconnected network of inhibitory neurons, representing the counterpart to the large number of excitatory neurons (Babaev et al. 2018b). However, their ability to orchestrate and control this flow is critically dependent on the transmission through chemical synapses. The synapse consists of a highly specialized and diverse molecular machinery of synaptic proteins at both the pre- and the postsynaptic terminal. While the precise functions of the continuously growing number of synaptic proteins are only just beginning to be elucidated, it is not surprising that mutations in these proteins may contribute substantially to the emergence of psychiatric disorders as they determine the physiological properties of synapses. Genetically modified mouse models have been developed and provide a valuable tool to study how synaptic proteins perturb synaptic function and how this subsequently affects behavior.

A prominent example for such a protein is the postsynaptic adhesion molecule and inhibitory synapse organizer Neuroligin-2 (Nlgn2), which is critical for inhibitory synapse maturation and maintenance (Varoqueaux et al. 2006; Poulopoulos et al. 2009). In line with the assumption that many neuropsychiatric disorders are synaptopathies (Hayashi-Takagi 2017; Wang et al. 2018), Nlgn2 has been associated with a variety of neuropsychiatric illness such as autism spectrum disorder (ASD), anxiety and schizophrenia (Ali et al. 2020).

Here we investigate the role of Nlgn2 in auditory cued fear conditioning (FC), a behavioral paradigm to investigate associative fear learning (LeDoux 2000; Fanselow und Poulos 2005). Excessive formation of fear memories as well as the burdening re-experience of those memories as flashbacks and resulting avoidance behaviors comprise the key symptoms of post-traumatic stress disorder (PTSD) in human patients. PTSD is a severe condition that can occur after a traumatic event of extraordinary magnitude, such as sexual violence or war, and which is often accompanied by substantial suffering pressure and the inability to withstand everyday life (Newport und Nemeroff 2000; Pitman et al. 2012). In addition, PTSD is highly comorbid with other mental illness including other anxiety disorders and major depression (Brady et al. 2000). Given that the options of pharmacological treatment are still limited and linked to unwanted side effects, it is crucial to understand why a subset of people develop PTSD while others form only few fear-related memories. This work based on a Nlgn2 knockout (KO) mouse model aims at identifying the neural circuits that are affected by Nlgn2 deletion and at characterizing the circuit mechanisms underlying the Nlgn2 KO

phenotype in auditory cued FC to in future provide a potential new target for specific cell-directed therapeutic approaches in the treatment of neuropsychiatric conditions such as PTSD.

1.1 Nlgn2 as a key component of the postsynaptic inhibitory machinery

Synapses are highly specialized subcellular compartments that are composed of both a machinery mediating neurotransmitter release and the respective receptors as well as a large and diverse group of scaffolding and organizational molecules. The four members of the neuroligin family that exist in mice (Nlgn1, 2, 3 and 4) belong to the latter group (Bemben et al. 2015). Their precise function arises from their differential localization at inhibitory and excitatory synapses. Nlgn1 was shown to be specific for excitatory synapses (Graf et al. 2004; Chih et al. 2005), whereas Nlgn3 is present at both inhibitory and excitatory synapses (Nguyen et al. 2020). While Nlgn4 was first associated with inhibitory synaptic transmission in rodents (Zhang et al. 2018), it has subsequently been shown to play a role in excitatory synapses in humans (Marro et al. 2019; Nguyen et al. 2020). Amongst all the members of the neuroligin family, Nlgn2 is unique as it was shown to exclusively localize across inhibitory synapses (Graf et al. 2004; Varoqueaux et al. 2004). Further, it plays a crucial role during the maturation as well as for maintenance of the inhibitory synapse (Ali et al. 2020). Taken together, these aspects make it a perfect candidate for studying the inhibitory synapse in health and disease.

1.1.1 Structure and interaction partners

Nlgn2, like all members of the neuroligin family, is a transmembrane protein consisting of a large extracellular domain at the mediating synaptic adhesion, a smaller intracellular domain as well as an α-helical transmembrane anchor (Ichtchenko et al. 1996). The extracellular domain at the N-terminal basically contains two different binding sites at opposite sides of the molecule (Koehnke et al. 2008). One site is crucial for Nlgn2 dimerization and highly conserved among all neuroligin family members, the other one is critical for neurexin (Nrxn) binding and clustering (Koehnke et al. 2008). To date, members of the Nrxn-family are the only known presynaptic interaction partners of Nlgn2 (Krueger et al. 2012) and it appears that the initial localization of Nlgn2 to the inhibitory synapse is governed by the splice form-specific binding to Nrxns (Nguyen et al. 2016).

The shorter intracellular domain at the C-terminal of Nlgn2 plays a key role in organizing postsynaptic protein clusters containing ɣ-aminobutyric acid-A receptors ($GABA_ARs$) and various types of scaffolding proteins (Krueger-Burg et al. 2017), such as gephyrin, the most extensively studied representative of the latter group. Nlgn2 was shown to accumulate at the synaptic sites due to its binding to presynaptic Nrxn molecules and to form tripartite complexes with gephyrin as well as the guanosine diphosphate/ guanosine triphosphate exchange factor collybistin which thereby changes its conformation to an active version enabling gephyrin to anchor $GABA_ARs$ (Poulopoulos et al. 2009; Papadopoulos und Soykan 2011; Soykan et al. 2014). Moreover, the intracellular domain of Nlgn2 also contains a binding site for PDZ domain-containing molecules like the scaffolding protein synaptic scaffolding molecule (S-SCAM) (Sumita et al. 2007). In addition to the functions mentioned above, the intracellular domain of Nlgn2 is also substantial for trafficking and endocytosis of Nlgn2 which is mediated by a direct interaction with the sorting nexin family member 27, preventing Nlgn2 from being decomposed in the lysosome and facilitating Nlgn2 recycling (Binda et al. 2019).

1.1.2 Role of Nlgn2 in protein composition across the inhibitory synapse

As reproduced in a variety of studies across several brain regions, Nlgn2 deletion particularly leads to a decreased amount of postsynaptic $GABA_ARs$ and gephyrin scaffolds, whereas the amount of proteins localized to the GABAergic presynapse such as the vesicular inhibitory amino acid transporter appears to be unaffected (Varoqueaux et al. 2006; Poulopoulos et al. 2009). These data indicate that the protein composition of the GABAergic post synapse is disturbed by Nlgn2 deletion, while the total number of inhibitory synapsed is not changed (Ali et al. 2020). Interestingly, Nlgn2 KO in the cornu ammonis 1 (CA1) region of the hippocampus leads to intracellular accumulations of gephyrin clusters, strengthening the notion that gephyrin recruitment to the postsynaptic membrane is disturbed in Nlgn2 KO mice (Poulopoulos et al. 2009).

1.1.3 Synapse-specific role of Nlgn2

Strikingly, it has been shown that constitutional KO of Nlgn2 in forebrain regions seems to particularly impair perisomatic synapses formed by parvalbumin-expressing (PV+) fast-spiking basket cells (Figure 1), even though Nlgn2 is present at nearly all inhibitory synapses (Ali et al. 2020). Consistent with this notion, the amount of gephyrin and $GABA_A$-receptor puncta in the basolateral amygdala (BLA) and hippocampus of Nlgn2 KO mice is decreased

in perisomatic regions, but not at the dendritic arbor of the neurons (Poulopoulos et al. 2009; Jedlicka et al. 2011; Babaev et al. 2016). However, the mechanisms leading to a synapse specific effect of Nlgn2 are still largely unknown and probably much more complicated than currently estimated, keeping in mind that the function of Nlgn2 may possibly be altered by synapse specific interactions with other synaptic proteins such as the immunoglobulin superfamily member 9b (IgSF9b) or the membrane-associated mucin domain-containing glycophosphatidylinositol anchor 1 and 2 (MDGA 1/2) (Ali et al. 2020).

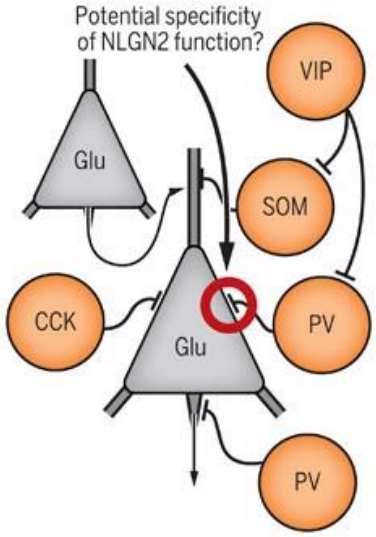

Figure 1: Proposed synapse specificity of Nlgn2 function. Nlgn2 deletion appears to mainly affect perisomatic synapses formed by PV+ basket cells. CCK, cholecystokinin: GLU, glutamate; PV, parvalbumin; SOM, somatostatin; VIP, vasoactive intestinal peptide. Adapted from (Ali et al. 2020). Reprinted with permission from AAAS.

1.2 Nlgn2 mutations in neuropsychiatric disease

Neuropsychiatric conditions are strongly linked to synaptic dysfunction, resulting in perturbance of the excitation/inhibition (E/I) ratio. Thus, given that Nlgn2 emerges as a central player in physiological GABAergic transmission, it is not surprising that Nlgn2 mutations in humans have been associated with mental disorders.

First, a genomic screening of a cohort of patients suffering from schizophrenia identified several rare missense mutations in the exons and promotor region of NLGN2 gene. Amongst these, the R215H mutation appeared to be pathogenic but only partially penetrant (Sun et al. 2011). As demonstrated with cell-based assays, the mutation leads to a loss-of-function protein due to failure in protein glycosylation and trafficking to the cell surface subsequently resulting in severe impairments of the inhibitory synaptic maturation (Sun et

al. 2011; Liang et al. 2015). In a more recent case report on a 15-year-old male patient showing a combination of ASD, anxiety, obsessive-compulsive disorder, obesity and macrocephaly, a heterozygous de novo nonsense mutation (Y147*) in NLGN2 gene was described which was predicted to contribute to the phenotype (Parente et al. 2017). Moreover, a genomic study revealed an increased level of rare mutations in mostly non-coding regions of NLGN2 gene (Curtis 2016). An enhanced expression of Nlgn2 has been observed in cortical interneurons of patients suffering from schizophrenia (Kathuria et al. 2019) as well as in nucleus accumbens of patients with depression (Heshmati et al. 2018). Last, mutations in several of the interaction partners of Nlgn2 have been linked to neuropsychiatric conditions in patients with partially overlapping phenotypes (Figure 2).

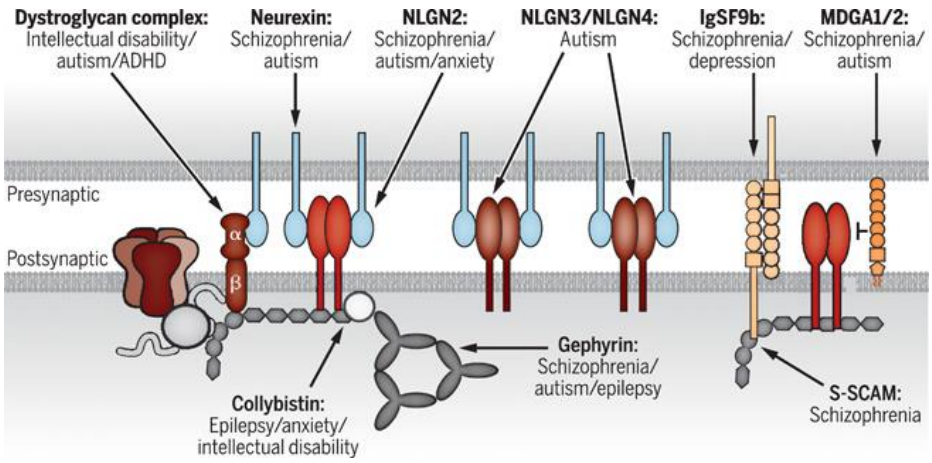

Figure 2: Nlgn2 and its interacting partners at the inhibitory synapse in neuropsychiatric disease. Mutations of Nlgn2 and its interaction partners neurexin (Nrxn) (Kasem et al. 2018), IgSF9b (Shyn et al. 2011; Schizophrenia Working Group of the Psychiatric Genomics Consortium 2014), dystroglycan complex (Waite et al. 2012) gephyrin (Lionel et al. 2013; Dejanovic et al. 2014), Nlgn3 and Nlgn4 (Kleijer et al. 2014), collybistin (Alber et al. 2017) , S-SCAM (Koide et al. 2012) and MDGA1/2 (Wang et al. 2019) have been associated with psychiatric disorders. Adapted from (Ali et al. 2020). Reprinted with permission from AAAS.

1.3 Nlgn2 function in aversive behaviors

Due to its key role in inhibitory synaptic transmission and in the maintenance of the balance of E/I ratio, Nlgn2 is also a particularly interesting candidate potentially contributing to aberrant behaviors. Thus, many studies on genetically modified rodents have focused on the role of Nlgn2 in specific behavioral outputs and neural circuits. So far, first evidence arose that Nlgn2 deletion may lead to a major impairment of behaviors involving an aversive component like fear and anxiety, which are amygdala-related behaviors, respectively (Table

1). In contrast, the impact on other behaviors seems to be surprisingly discrete (Ali et al. 2020).

One of the most prominent characteristics in the behavior of the global Nlgn2 KO mice is the robust anxiety-like phenotype which has been observed in approach avoidance paradigms. Interestingly, recent studies provide evidence that overexpression of Nlgn2 also results in increased freezing levels, strengthening the notion that a disturbance of the E/I balance in either way may lead to pronounced avoidance behaviors (Hines et al. 2008).

Astonishingly few studies have investigated the role of Nlgn2 within neural circuits underlying cognitive function and hence little is known about it to date. However, the existing studies indicate that learning processes with an aversive component are particularly affected (Ali et al. 2020). For instance, conditional Nlgn2 KO in the mPFC resulted in a deficit in fear retrieval in both contextual and cued FC paradigms (Liang et al. 2015).

Further, Nlgn2 deletion does not seem to have any major consequences either on sensory functions or on the motor behavior. Especially auditory function showed no deficits in Nlgn2 KO mice compared to wild type (WT) mice, as assessed by a tone discrimination task (Chen et al. 2019) and by the startle response test (Wöhr et al. 2013).

Table 1: Effect of Nlgn2 manipulations on associative fear learning.

Behavior	Nlgn2 manipulation	Effect on behavior	Reference
Fear	cNlgn2 KO in mPFC	↓ contextual and cued FC	(Liang et al. 2015)
	cNlgn2 KO in NR	↓ contextual discrimination in FC	(Xu und Südhof 2013)
	Nlgn2 inhibition in mPFC	↓ memory retention in inhibitory avoidance paradigm	(Ye et al. 2017)
	Nlgn2 KO	↓ avoidance of a punished tone in an auditory discrimination task	(Chen et al. 2019)

This table summarizes the consequences of Nlgn2 manipulations on fear-related behaviors that have been observed. ↑, increase; ↓, decrease; ↔, no change; Nlgn2, Neuroligin-2; KO, knockout; cNlgn2 KO, conditional Nlgn2 KO; mPFC, medial prefrontal cortex; BLA, basolateral amygdala; FC, fear conditioning; NR, nucleus reuniens. Adapted from (Ali et al. 2020).

1.4 Brain regions in auditory fear processing

As outlined in detail above, Nlgn2 mutations are associated with a large variety of neuropsychiatric conditions in human patients and, in addition, were shown to affect defensive behaviors in rodents (Table 1) (Ali et al. 2020). Hence, the arising question is how Nlgn2 deletion mechanistically affects defensive behaviors and a precondition to understand this is a profound knowledge of the fear-processing network, which will be introduced below.

1.4.1 The role of the amygdaloid complex in the processing of fear

One of the key regions in orchestrating dynamic adaptive behaviors to emotional states with an aversive component like fear or anxiety is the amygdala, an evolutionarily highly preserved complex of several nuclei which is located within the temporal lobe (Janak und Tye 2015). Anxiety and fear are processed by different, albeit partially overlapping networks (Tovote et al. 2015) and one needs to bear in mind that they are distinct conditions: Fear is an acquired reaction to a threat that requires rearrangement of neural circuits, whereas anxiety is an innate behavior mediated by existing circuits (Tovote et al. 2015; Craske und Stein 2016). While little is known about anxiety networks yet, fear-processing circuits were studied much more intensively and are hence better understood.

Regarding fear circuits, mainly two nuclei within the amygdaloid complex play a prominent role: The BLA and the central amygdala (CeA), which can be further subdivided into the lateral (LA) and the basal amygdala (BA) as well as into the centrolateral (CeL) and the centromedial amygdala (CeM) (Janak und Tye 2015). The most accepted, but presumably too simplified model on the flow of information throughout the amygdala (Figure 3 A) is that projections from upstream areas like the auditory cortex (AuC) or the medial prefrontal cortex (mPFC) reach the amygdala particularly through the LA (Tovote et al. 2015). A large variety of studies provide evidence that the LA is crucial for formation and retrieval of fear memories (LeDoux 2000; Johansen et al. 2010; Amano et al. 2011) and that associative plasticity in LA is decisive for fear learning (Rogan et al. 1997; Rosenkranz und Grace 2002; Nabavi et al. 2014). After arriving in the LA, the signal is processed in the BA and follows the pathway to finally reach the CeA (Babaev et al. 2018b). Last, the information is projected to downstream areas via the CeM which in turn receives tonic inhibitory afferents from the CeL (Ciocchi et al. 2010). Although the CeM is considered the main output nucleus of the amygdaloid complex (LeDoux et al. 1988), a growing body of evidence arose from several studies that the CeL also has long range projections targeting downstream effector regions

that mediate freezing responses such as the periaqueductal grey (PAG) (Vianna et al. 2001; Penzo et al. 2014; Tovote et al. 2016). These data implicate that the CeL directly modulates fear behavior independently from the pathway that conveys the information through the CeM (Penzo et al. 2014).

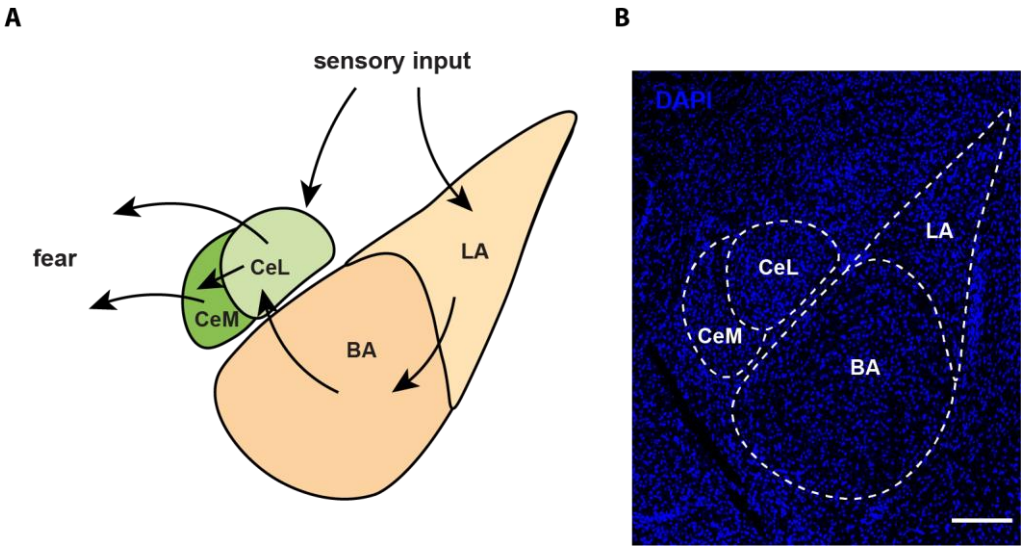

Figure 3: Model on the flow of information throughout the amygdala. Schematic model on fear processing within the amygdala. **B)** Immunohistochemical overview of the amygdaloid complex. Scale bar = 200 µm. Figure created after (Ehrlich et al. 2009) with permission from Elsevier.

1.4.2 The role of the mPFC in the processing of fear

Even though the amygdala presumably lies in the center of the fear circuit, it is embedded in a brain wide fear-processing network including various up- and downstream regions. Amongst these, the mPFC has emerged as a key region that is critically implicated in modulating the expression of acquired fear (Courtin et al. 2013). The mPFC is composed of two subregions, the prelimbic cortex (PrL) and the infralimbic cortex (IL), both of which are highly interconnected with a wide range of brain regions, including the medial-dorsal thalamus (Uylings und van Eden 1990), the hippocampus (Swanson 1981) and the BLA (McDonald 1987). Pre- and post-FC training inactivation of the PrL lead to a reduction of fear expression (Corcoran und Quirk 2007; Sierra-Mercado et al. 2011), whereas the same manipulations on the IL did not have an effect on fear expression, but interfered with fear extinction learning (Laurent und Westbrook 2009; Sierra-Mercado et al. 2011). Consistently, BA-PrL projections were shown to be strongly activated during fear acquisition, while IL-projecting neurons within the BA showed enhances activation during extinction (Senn et al. 2014). Taken together, these data indicate that both regions play dissociable roles in fear

learning and that the strength of a conditioned fear memory may be modulated by shifts in the balance of activation of PrL-BA and IL-BA pathways (Gafford und Ressler 2016).

1.4.3 The role of the AuC in auditory FC

When investigating auditory cued fear memories, it is of particular interest to understand how the auditory information and the threatening foot shock become associated among one another to induce learning processes that are finally translated into behavior. While the critical role of synaptic plasticity within the LA in pavlovian FC has been studied extensively and is established by a wide range of studies (Tovote et al. 2015), a growing body of evidence further supports a key role of the AuC in encoding the emotional meaning of sounds (Grosso et al. 2015; Concina et al. 2019). It was already possible to show decades ago that pairing of a sound with an emotional incident causes a robust cortical rearrangement (Quirk et al. 1997; Armony et al. 1998). However, this finding has long been assumed reflecting pure stimulus properties, rather than being due to local associative learning linking a tone with an emotional valence and specific behavior (Aschauer und Rumpel 2018). In contrast, more recent studies were able to demonstrate that AuC neurons are highly activated by foot shocks and other painful stimuli without any presentation of tones (Letzkus et al. 2011; Peter et al. 2012) and that plasticity in AuC neurons is required for auditory FC (Letzkus et al. 2011). These findings strongly indicate that AuC circuits underlie plastic modifications induced by the convergence of the conditioned tone and its aversive consequences (Letzkus et al. 2015) and that, apart from simply carrying the auditory information, they are critically implicated in the mechanisms of associative fear learning.

1.5 Neuronal populations in amygdala fear circuits

As discussed above in detail, two main complexes of the amygdala, the BLA and the CeA, are critical for associative fear learning. However, these two nuclei derive from entirely different cellular origins, particularly regarding inhibitory neuronal populations. The BLA is considered a cortical-like structure consisting of up to 80% of excitatory pyramidal cells and only of approximately 20% of inhibitory interneurons (McDonald 1985; Sah et al. 2003; Rainnie et al. 2006; Spampanato et al. 2011). In contrast, the CeA is a striatal-like structure consisting almost exclusively of different subtypes of GABAergic inter- and projection neurons (Sah et al. 2003; Janak und Tye 2015).

1.5.1 Inhibitory interneurons in BLA

The firing of BLA glutamatergic projection neurons is tightly regulated via feedforward and feedback inhibition provided by local inhibitory microcircuits (Spampanato et al. 2011) which are still not entirely understood. BLA GABAergic interneuron projections are usually restricted to the BLA (McDonald 1985; Kemppainen und Pitkänen 2000) and they can be classified into two non-overlapping groups dependent on their expression of two distinct calcium-binding proteins, calretinin and calbindin (Capogna 2014). The most important representatives of the latter group accounting for approximately 60% of BLA interneurons are either immunoreactive for PV, for somatostatin (SOM+) or for cholecystokinin (CCK+). Calretinin-expressing interneurons can be further subdivided into vasoactive intestinal peptide-expressing (VIP+) neurons and CCK+ neurons, albeit these groups partially overlap (Kemppainen und Pitkänen 2000; Mascagni et al. 2009).

PV+-neurons preferentially target BLA principal neurons forming baskets around their soma and the proximal dendrites, but there is also a small subgroup of axoaxonic cells. Moreover, the axonal arbor of PV+ interneurons also targets SOM+ cells and forms many synapses onto other PV+ cells, forming a network potentially maintaining regulatory gamma oscillations as observed in cortical areas (Muller et al. 2005; Buzsáki und Wang 2012). In contrast, SOM+ neurons regulate glutamatergic projection neurons by mainly targeting their distal dendrites, while they, in turn, receive dampening inputs from PV+ neurons. This microcircuit allows the disinhibition of BLA principal neurons via feedforward inhibition of SOM+ cells provided by PV+ interneurons (Muller et al. 2007; Wolff et al. 2014; Babaev et al. 2018b) and has been shown to control freezing levels in auditory cued fear conditioning paradigms. Consistent with this finding, optogenetic activation of SOM+ interneurons lead to pronounced freezing responses (Wolff et al. 2014). Recently, it has been demonstrated that VIP+ neurons within the BLA exhibit strongly enhanced neural firing during fear acquisition and that this is an obligatory signal to induce the formation of fear memories (Krabbe et al. 2019). Inhibition of VIP+ neurons during presentation of the aversive stimulus only little affected somatic responses of pyramidal neurons, but strongly interfered with responses to the conditioned tone (Grewe et al. 2017). Together, these data indicate that VIP+ neurons enable the disinhibition of pyramidal neurons during fear learning through inhibition of SOM+ neurons targeting their dendritic arbor (Krabbe et al. 2019). Similar to their connectivity in cortical circuits (Pfeffer et al. 2013; Pi et al. 2013), VIP+ neurons within the BLA were shown to mainly project onto other interneurons including PV+, SOM+ cells as well as onto other VIP+ neurons, but a smaller subpopulation also directly targets

principal neurons around their soma (Rhomberg et al. 2018). In addition, there is evidence for a strong reciprocal interconnection of BLA interneurons, suggesting that inhibitory interneurons may change their activation patterns in a contextual manner and thereby permit flexible behavioral responses (Krabbe et al. 2019).

1.5.2 Inhibitory neuronal populations in CeA

The role of local inhibitory microcircuits is particularly prominent in CeL (Tovote et al. 2015; Babaev et al. 2018b). In contrast, comparable networks have not yet been identified in the CeM , whose GABAergic neurons are thought to mainly mediate fear-related behaviors via downstream projections (Ciocchi et al. 2010).

The inhibitory neuronal population within CeL consists of two distinct groups either protein kinase δ-expressing (PKC-δ+) or SOM+ neurons (Haubensak et al. 2010; Gilpin et al. 2015; Hunt et al. 2017). Chemokinetic suppression of CeL SOM+ neurons before FC lead to impaired fear acquisition and activation of SOM+ cells provoked freezing in naive animals (Li et al. 2013). Together, these data implicate that SOM+ neurons in CeL are crucial for both fear learning and fear expression and highlight their role in directly modulating behavioral outputs, as they do not project to CeM projection neurons but entirely bypass them (Penzo et al. 2014). Regarding PKC-δ+ neurons, previous studies pursuing optogenetic approaches found that they send out tonic inhibitory signals onto CeM projection neurons (Ehrlich et al. 2009; Haubensak et al. 2010). Optogenetic activation of PKC-δ+ reduced the activity of CeM projection neurons to the PAG. The inhibition of PKC-δ+ neurons, in turn, lead to higher freezing levels, indicating that they gate freezing by tonically inhibiting the CeM output (Haubensak et al. 2010). It is widely assumed that SOM+ neurons regulate PKC-δ+ neurons in their activity (Babaev et al. 2018b) and consistent with this notion, optogenetic activation of SOM+ neurons provokes freezing in unconditioned mice (Fadok et al. 2017).

In contrast to the CeL, much less is known about inhibitory neurons in CeM. So far, three groups of neurons expressing either SOM, tachykinin 2 (Tac2) or neurotensin have been identified (Kim et al. 2017), but their precise role in the fear circuit remains to be determined. In the few existing studies on CeM inhibitory neurons it was shown that chemogenetic activation of Tac2+ neurons in unconditioned mice provoked freezing-like behavior (Kim et al. 2017) and, consistently, inhibition of Tac2+ neurons before FC resulted in reduced freezing behavior (Andero et al. 2014).

1.6 Aim of the project

Pursuing a top-bottom approach, this project aims to investigate the implications of the synaptic adhesion molecule Nlgn2 in the cellular and molecular mechanisms underlying associative fear learning and, thus, to shed a light on pathological circuit function in fear-related disorders such as PTSD. After the characterization of the Nlgn2 phenotype in auditory cued FC, two main questions were addressed:

1. How does Nlgn2 deletion affect the activation pattern within fear-related brain areas, and which region is likely contributing to the Nlgn2 phenotype in FC?

2. Which subtypes of GABAergic neurons are affected by Nlgn2 deletion and may therefore contribute to the behavioral phenotype of Nlgn2 KO mice?

To address these questions, I conducted a cFos induction assay after auditory cued FC. cFos is a proto-oncogene with a low baseline expression in neurons which is strongly and transiently upregulated in response to an increase in the intracellular concentration of free calcium due to enhanced depolarization (Morgan und Curran 1988). Therefore, cFos belongs to the heterogenous group of immediate early genes (IEGs) and the quantification of cfos-expressing nuclei is a well-established method to visualize and measure neuronal activity (Sagar et al. 1988). First, I characterized the activation patterns of the amygdaloid complex, the mPFC, the ventrolateral PAG (vlPAG) and the AuC by quantification of the overall cFos expression. Second, I co-labeled for cFos and inhibitory cellular markers to dissect the different neuronal subpopulations. Last, I started establishing retrograde anatomical tracing through stereotactic microinjections of a retrograde tracer into the LA.

2 Material and methods

2.1 Materials

Table 2: List of equipment.

Fear conditioning	
Equipment	Company
Cued fear conditioning setup	Med Associates inc., St. Albans, USA
Immunohistochemistry	
Equipment	Company
Leica CM3050 S cryostat	Leica Biosystems, Wetzlar, Germany
Leica SP8 confocal microscope	Leica Biosystems, Wetzlar, Germany
Perfusion pump	Rottenberg Laborgeräte, Germany
Surgeries	
Equipment	Company
Curved hemostat	Fine science tools, Heidelberg, Germany
Drill	World Precision Instruments, Sarasota, USA
Ear bars	World Precision Instruments, Sarasota, USA
Forceps	Fine science tools, Heidelberg, Germany
Hamilton syringe (1 µl)	Hamilton company, Reno, USA
Dino-lite Microscope	Sotac Computer GmbH, Stuttgart, Germany
Mouse adaptor	World Precision Instruments, Sarasota, USA
Probe holder	World Precision Instruments, Sarasota, USA
Scalpel	Fine science tools, Heidelberg, Germany
Scissors	Fine science tools, Heidelberg, Germany
Stereotaxic frame	World Precision Instruments, Sarasota, USA

Table 3: List of materials.

Material	Company
Butterfly needles	Servoprax, Wesel, Germany
Cannulas 20 G, 27 G	Becton Dickinson, Franklin Lakes, USA
Cellstar® tubes 15 ml	Greiner, Frickenhausen, Germany
Cotton swabs	Glaswarenfabrik Karl Hecht, Sondheim, Germany
Eppendorf tubes® 0.5 ml	Eppendorf, Hamburg, Germany
Falcon tubes® 50 ml	Corning Science, New York, USA
Filter System 500 ml	Corning Science, New York, USA
Lens cleaning tissue	GE Healthcare, Chicago, USA
Microscope wipes	Kimberly-Clark, Dallas, USA
pipette tips 10 µl, 200 µl, 1000 µl	Thermo Fischer Scientific, Waltham, USA
Surgical sutures	Johnson & Jonson, Livingston, UK
Syringe 1 ml	Becton Dickinson, Franklin Lakes, USA
Syringe-driven filters	Merck Millipore, Burlington, USA
24-well plates	Greiner, Frickenhausen, Germany

Table 4: List of chemicals.

Immunohistochemistry	
Substance	Company
2-metyl-2-butanol	Sigma-Aldrich, St. Louis, USA
2,2,2-Tribromethanol	Thermo Fischer Scientific, Waltham, USA
Aqua-Poly/Mount	Polysciences, Hirschberg, Germany
Bovine serum albumin (BSA)	Biomol, Hamburg, Germany
Di-sodium hydrogen phosphate dihydrate	Merck Millipore, Burlington, USA
Immersion oil	Carl Zeiss, Oberkochen, Germany
Normal goat serum (NGS)	Life Scientific, Dublin, Irland
Sucrose	Sigma-Aldrich, St. Louis, USA
Paraformaldehyde	Serva, Heidelberg, Germany
Potassium chloride	Merck Millipore, Burlington, USA
Potassium dihydrogen phosphate	Merck Millipore, Burlington, USA
Sodium chloride	Merck Millipore, Burlington, USA
Sodium dihydrogen phosphate monohydrate	Merck Millipore, Burlington, USA
Tissue-Tek®	O.C.T. Compound Science Services, Düsseldorf, Germany
Triton X-100	F. Hoffmann-La Roche, Basel, Schweiz

Surgeries	
Substance	Company
Carprofen (50 mg/ml)	TAD pharma, Cuxhaven, Germany
Ethanol (70 %)	Sigma-Aldrich, St. Louis, Missouri, USA
Iodine	aniMedica, Senden-Bösensell, Germany
Isofuorane (1 ml/ml)	CP-Pharma, Burgdorf, Germany
Lidocain (20 mg/ml)	Richter pharma, Wels, Austria
Metamizol (500 mg/ml)	Ratiopharm, Ulm, Germany
RetroBeads™ (emission max. 530 nm)	Lumafluor, Durham, USA
Saline (sterile, 0.9 % NaCl in ddH_2O)	
Vaseline	Lenhart Kosmetik, Waiblingen, Germany

Table 5: List of primary antibodies.

Primary antibodies					
Antigen	Species	Dilution	Duration of incubation	Catalogue number	Company
cFos	guinea pig, polyclonal	1:2000	12 h	226 005	Synaptic Systems, Göttingen, Germany
GFP	rabbit, polyclonal	1:500	12 h	123 003	Synaptic Systems, Göttingen, Germany
	guinea pig, polyclonal	1:500	12 h	123 005	Synaptic Systems, Göttingen, Germany
PKC-δ	Mouse, monoclonal	1:2000	12 h	610398	BD transduction laboratories, NJ, USA
PV	rabbit, antiserum	1:5000	12 h	PV27	SWANT, Bellinzona, Switzerland
SOM	mouse, monoclonal	1:500	12 h	sc-55565	Santa Cruz Biotechnology, Dallas, TX, USA
VIP	Rabbit, antiserum	1:500	12 h	20077	Immunostar, WI, USA

Table 6: List of secondary antibodies.

Secondary antibodies		
Fluorophore	Species	Company
Alexa 488	goat anti-rabbit	Life Technologies, CA, USA
	goat anti-guinea pig	Life Technologies, CA, USA
	goat anti-mouse	Invitrogen Eugene, OR, USA
Alexa 555	goat anti-mouse	Invitrogen Eugene, OR, USA
Alexa 633	goat anti-guinea pig	Life Technologies, CA, USA

All secondary antibodies were incubated for 2-3 h in 1:600 dilution with blocking buffer.

All antibodies used in this study were optimized regarding their concentration and staining conditions prior to the actual experiments.

The anti-cFos antibody (#226 005, Synaptic Systems, Göttingen, Germany) was raised against rat cFos and purified with the immunogen. It is frequently used in publications (Gu et al. 2020; Pan-Vazquez et al. 2020) and is compatible with paraformaldehyde (PFA) fixation. Importantly, since this antibody is our main measurement tool, we validated it ourselves before conducting the experiments, which will be demonstrated in the results part of this work.

The rabbit anti-PV antibody (PV27, SWANT, Bellinzona, Switzerland) was raised against recombinant rat PV and the manufacturer demonstrates that it clearly labels PV+ cells in cerebellar tissue of WT mice, whereas there is no specific staining in PV KO mice (https://www.swant.com/pdfs/PV27_Rabbit_anti_Parvalbumin.pdf).

The specificity of the rabbit anti-VIP antibody (#20077, Immunostar, WI, USA) was characterized by VIP pre-adsorption test which eliminated VIP immunolabeling (Sloviter und Nilaver 1987). Following the manufacturer information, pre-adsorption test with other peptides such as SOM, substance P and neuropeptide Y did not reduce the immunolabeling (https://www.immunostar.com/product/vip-vasoactive-intestinal-peptide-antibody/). In addition, it is commonly used for immunohistochemical studies on PFA-fixed tissue containing the mouse BLA (Rhomberg et al. 2018; Krabbe et al. 2019) as well as various other brain regions (Mazuski et al. 2020).

The mouse anti-PKC-δ antibody (#610398, BD transduction laboratories, NJ, USA) was purified by affinity chromatography. Further, it is used in recent publications (Hunt et al. 2017).

The mouse anti-SOM antibody (sc-55565, Santa Cruz Biotechnology, Dallas, TX, USA) was raised against human SOM and was also used in previous publications (Babaev et al. 2016; Chen et al. 2020).

Table 7: List of solutions.

Solution	Composition
Avertin	125 µl Avertin, 350 µl EtOH, 4500 µl saline; total volume 5 ml
Avertin stock solution	5 g 2,2,2-Tribromoethanol in 5 mL methyl-2-butanol
Blocking buffer	5 ml NGS, 1.5 ml Triton X-100 (10%), 1.5 g BSA in PBS; total volume 50 ml
PFA, 4%	40 g of paraformaldehyde in 0.1 M PB; total volume 1 L
Phosphate buffer (PB), 0.2 M	27.3 g of Na_2HPO_4, 7.36 g of NaH_2PO_4 in ddH_2O; total volume 1 L; pH= 7.4
Phosphate-buffered saline (PBS)	160 g of NaCl, 4.0 g KCl, 36.1 g of Na2HPO4*2H2O, 4.8 g KH2PO4 in ddH_2O; total volume 2 L; pH= 7.4
Saline, 0.9%	9 g of NaCl in 1000 ml ddH_2O
Sucrose solution, 30%	30 g of sucrose in 0.1 M PB; total volume 100 ml

Table 8: Software.

Software	Company	Application
Illustrator	Adobe Inc., San José, USA	Creation of figures
Excel	Microsoft, Redmond, USA	Quantification sheets
Prism	GraphPad Sofware Inc., La Jolla, USA	Statistical analysis
ImageJ (Fiji)	NIH (open source)	Image processing
Imaris	Bitplane, Zürich, Switzerland	Image quantification
VideoFreeze®	Med Associates Inc., St. Albans, USA	Behavioral characterization

2.2 Experimental animals

All experiments were conducted at the Max Planck Institute of Experimental Medicine in accordance with the animal welfare laws of the Federal Government of Germany and the corresponding guidelines of the Max Planck Society. All procedures were approved by the

State of Niedersachsen (Landesamt für Verbraucherschutz und Lebensmittelsicherheit, TVA 33.19-42502-04-20/3368).

Nlgn2 KO mice (Varoqueaux et al. 2006) were generated on a 129/Sv background and backcrossed onto a C57BL/6JRj background for at least six generations in the animal facility of the Max Planck Institute of Experimental Medicine. Male Nlgn2 KO and WT mice were obtained from Nlgn2 heterozygous breeding pairs. PV-Internal Ribosome Entry Site (IRES)-Cre (Hippenmeyer et al. 2005), SOM-IRES-Cre, VIP-IRES-Cre mice (Taniguchi et al. 2011) and CAG-CAT-EGFP mice (Nakamura et al. 2006) were obtained from The Jackson Laboratory, Sacramento, and they were backcrossed onto a C57BL/6JRj background for at least four generations in the animal facility of the Max Planck Institute of Experimental Medicine. The IRES-construct is a technical strategy that permits the expression of two proteins, e.g. Cre and PV, SOM or VIP, from one promoter in eukaryotes. To generate Cre driver mice that selectively express enhanced green fluorescent protein (EGFP) in PV+, SOM+ and VIP+ neurons, the respective IRES-Cre line was crossed with the CAG-CAT-EGFP line. Mice were at the age of six-eight weeks when they received surgeries and two-three months old when they were included in a behavioral experiment. Animals were housed in groups and maintained on a 12-hour light/dark cycle. They were provided with food and water *ad libitum*. During all steps of data acquisition and analysis, the experimenter was blinded to the genotype and the treatment of the mice.

Table 9: List of mouse lines.

Mouse line	Source	Reference
CAG-CAT-EGFP	The Jackson Laboratory, Sacramento, USA	(Nakamura et al. 2006)
Nlgn2 KO	MPI of Experimental Medicine, Göttingen, Germany	(Varoqueaux et al. 2006)
PV-IRES-Cre	The Jackson Laboratory, Sacramento, USA	(Hippenmeyer et al. 2005)
SOM-IRES-Cre	The Jackson Laboratory, Sacramento, USA	(Taniguchi et al. 2011)
VIP-IRES-Cre	The Jackson Laboratory, Sacramento, USA	(Taniguchi et al. 2011)

2.3 Behavioral characterization

Auditory cued FC is a robust and well-established behavioral paradigm to investigate associative fear learning. An initially neutral stimulus, in this case a tone, is associated with an aversive component, a foot shock which is also called the unconditioned stimulus (US), by classical Pavlovian conditioning and thereby becomes the conditioned stimulus (CS). To induce the learning process, mice are repetitively exposed to tone-shock sequences. 24 h after the training, freezing levels in response to presentation of the CS are measured to evaluate the ability of the respective animal to acquire, consolidate and retrieve the fear memories. Freezing is defined as the absence of movement except for breathing, and even though it is only a binary behavior (the animal freezes or it does not), it is accepted as a valuable and reliable tool that, in addition, can be assessed quite easily, especially in contrast to other fear responses such as offensive or flight behaviors.

The FC paradigm used for this study was conducted within 2 days (Figure 6 A). On training day, mice were single housed 2 h prior to the experiment. After the mouse was placed in the FC chamber, it had 2 min to explore the novel environment and baseline freezing was measured. Subsequently, depending on whether the animal underwent fear conditioning or served as control, either two tone-shock sequences or only the tones were presented at an interval of 60 sec. During one sequence, the tone (80 dB, 5 kHz) was presented for 30 sec and, for animals that received paired training, combined with foot shock (0.5 mA, 2 sec, co-terminating with the tone). Finally, after another 30 sec, the mouse was removed from the FC chamber and placed back in its home cage. FC testing was conducted 24 h later. For that purpose, mice were immediately transferred from the mouse hotel to the behavior room. The testing chamber was cleaned with ethanol and baseline freezing was quantified during the two minutes of habituation. Then, the CS was presented to conditioned and control animals and freezing levels were measured for 30 sec during the presentation of the tones. Freezing was assessed using VideoFreeze® software and was defined as no movement for 7 consecutive frames at a rate of 15 frames/ second.

To reduce contextual fear learning, the stimuli were presented in distinct contexts on training and testing day. For instance, environmental factors like the light-dark situation, the shape of the FC chamber, the material of our gloves and the cleaning agent were changed between both days.

Mice underwent FC in sets of four animals which were kept constant from the behavior through all steps of data analysis to ensure constant experimental conditions for animals that

were statistically compared among each other. One set of four mice was composed of a Nlgn2 KO and a WT animal that received paired FC training, as well as of controls for both genotypes, which were only exposed to the CS, but not to the foot shock on training day.

2.4 Perfusion fixation

Quantification of IEG cFos-expressing neurons was used to investigate the activation of fear-related brain regions in WT and Nlgn2 KO mice after retrieval of the auditory cued fear memories. To allow cFos expression that reaches its peak 90-120 min after presentation of the stimulus (Numan und Numan 1994; Chaudhuri et al. 2000), mice were anaesthetized with Avertin (dosage 50 µl/25 g bodyweight) 90 min after exposure to the CS on testing day. Subsequently, they were perfused transcardially with 0.9% saline for 1 min and with 4% PFA in 0.1 M PB for 8 min with decreasing speed. Dissected and fixed brains were stored overnight at 4°C in 4% PFA solution for post fixation and afterwards transferred to 30% sucrose in 0.1 M PB for cryoprotection. Before further processing, brains were kept for at least 3 days at 4°C to ensure that they are entirely saturated with the sucrose.

2.5 Immunohistochemistry

Free-floating coronal sections of 40 µm thickness were cut with a Leica CM3050 S cryostat at -20°C and collected in 1% phosphate buffered saline (PBS) of pH 7.4. After blocking for 2 h in blocking buffer (10% normal goat serum (NGS), 0.3% Trition-X and 3% bovine serum albumin (BSA) in PBS), slices were incubated with primary antibodies diluted in blocking buffer in respective optimized concentration (Table 5) overnight (12-24 h) at 4°C and afterwards conjugated with secondary antibodies diluted 1:600 for 1.5 hours at room temperature. Nuclei were labeled with 4',6-diamidino-2-phenylindole (DAPI) in 1:10000 dilution in PBS for 10 min. Slices were washed three times for 10 min with PBS after every staining step. Brain slices of four animals constituting one set of mice that were compared among each other were stained during the same staining session. Finally, the slices were mounted on glass slides and coverslipped using Aqua-Poly/Mount. After 24 h, the curing process of the mounting medium was completed, and the samples were prepared for imaging.

2.6 Image acquisition

Overview images of the amygdaloid complex, the mPFC, the AuC and the vlPAG were acquired with a Leica SP8 confocal microscope using a 20x immersion objective at a 512 x 512 format. The acquisition speed was set to 600 in a bidirectional scan mode, the zoom factor to 1 and the fluorescent signal was averaged four times line by line. A sequential scan of four channels was conducted. The lasers were set to the following excitation values of 633 nm (cFos), 555 nm (SOM and PKC-δ), 488 (VIP and PV), 530 (RetroBeads™) and 405 nm (DAPI). For each image, two optical sections with a stack thickness of 3 µm were recorded. Imaging parameters e.g., laser output, offset and gain were kept constantly while imaging one set of four mice which were statistically compared and normalized to each other. For the general cFos analysis, eight images per region and animal with different distances from bregma were anatomically matched and averaged. For the cell-specific analysis, four pictures with different distance from bregma containing all subnuclei of the amygdala (Table 10) were averaged per animal and cell type.

Table 10: List of assessed brain regions with anterior/posterior coordinates from bregma.

Brain region	Subregion	Distance from bregma
Amygdala	BA	-0.58 mm - -1.82 mm
	CeL	-1.22 mm - -1.94 mm
	CeM	-0.58 mm - -1.58 mm
	LA	-0.70 mm - -1.82 mm
Auditory cortex	Au1, AuV, AuD	-2.06 mm - -3.64 mm
Medial prefrontal cortex	IL	1.98 mm - 1.34 mm
	PrL	2.46 mm - 1.54 mm
Ventrolateral periaqueductal grey	PAG	-4.16 mm – 5.20 mm

Coordinates according to: (Paxinos und Franklin 2001)

2.7 Image processing and analysis

Image processing and quantification of cFos puncta were conducted in ImageJ (Fiji) and Imaris (Bitplane) (Figure 4). Images were first loaded to ImageJ (Fiji) to define regions of interest by outlining the relevant brain regions. The threshold was calculated by manually choosing an area of higher background and an area of lower background signal, averaging the two intensities, and multiplying the obtained value by three. Both processing steps were automized with respective macros. Entirely processed images were loaded to Imaris and the number of cFos+ cells within the different anatomical locations was quantified with the "spots" function. Colocalization analysis of cFos expressing nuclei and cellular markers was done with the "colocalize spots" function in Imaris (Figure 5). The respective parameters for spots creation for each marker are specified below (Table 11).

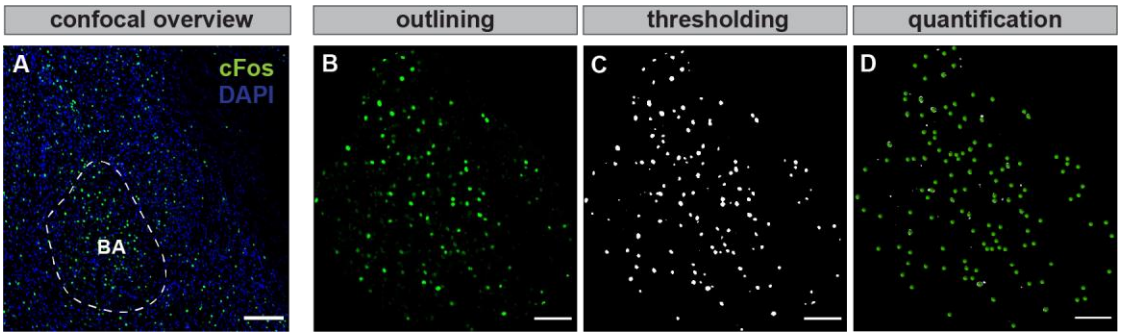

Figure 4: Representative photomicrographs illustrating the cFos quantification strategy. A) Confocal overview image of the amygdaloid complex. The outlining around the BA demonstrates how regions of interest were determined. Scale bar = 200 μm. **B-C)** Image processing in ImageJ (NIH) with respective macros. First, the defined region of interest was cut out and the DAPI channel was removed (B). Second, based on the background intensity, a thresholded mask was created (C). Scale bar = 50 μm. **D)** cFos quantification using "create spots" function in Imaris software (Bitplane). Scale bar = 50 μm.

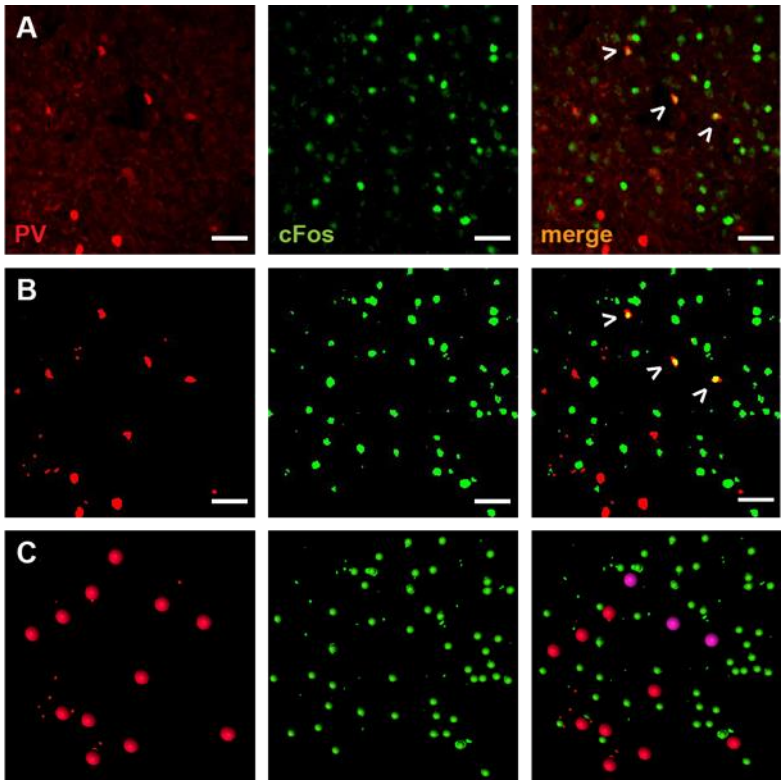

Figure 5: Photomicrographs demonstrating the quantification strategy for cell type-specific cFos quantification. A) Upper row: Confocal photomicrographs of PV+ cells and cFos in BA. **B)** Middle row: Images were loaded to ImageJ for thresholding. Arrow heads mark double-labeled cells. Scale bar = 50 µm. **C)** Lower row: Colocalization analysis and quantification were performed using "colocalize spots" function in Imaris. Purple spots mark double-labeled neurons.

Table 11: Parameters for image analysis in Imaris.

Marker	Diameter	Quality threshold	Distance threshold for colocalization with cFos
cFos	12 µm	20	-
PKC-δ	13 µm	30	5 µm
PV	22 µm	6	5 µm
SOM	15 µm	20	10 µm
VIP	15 µm	15	5 µm

2.8 Stereotactic surgeries and retrograde tracing

First, mice were placed in an induction chamber and anesthetized with 4% Isoflurane in 1 L/min O_2, followed by a maintenance dosage of 1% Isoflurane and were injected intraperitoneally with carprofen (5 mg/kg). Protecting ointment was applied onto the eyes immediately after the anesthetic drugs showed an effect. After confirming the depth of anesthesia by testing the pinch-reflex, mice were fixed in a stereotactic frame and an anterior-posterior incision was made. Then, lidocaine was locally applied, and the scull was aligned horizontally. To prevent the tissue from drying, the exposed scull was continuously moisturized with saline during the whole surgical procedure. Burr holes were drilled and 75 nl of red fluorescent RetroBeads™ (excitation max. 530 μm, emission max. 590 μm) were injected bilaterally into the LA (-1.1 A/P, ± 3.5 M/L, -3.8 D/V from the scull surface) at a rate of 0.5 nl/sec using a Hamilton syringe (1 μl). RetroBeads™ are fluorescent latex particles that enter the neuron through its presynapse to subsequently travel up the axon and finally accumulate inside the cell bodies. To reduce backflow and allow diffusion of the RetroBeads™, the tip of the syringe was left in place for 5 minutes after the injection was finished, then withdrawn for 100 μm and left in place for another three minutes before being entirely withdrawn at a rate of 1 mm/minute. Finally, the skin was sutured and iodine was applied to disinfect the wound. For rehydration, mice were injected intraperitoneally with 0.3 ml of isotonic saline before they were brought back to their home cages which were placed on a heating pad overnight. To reduce post-surgical pain, mice were provided with Metamizol (200 mg/kg/day) in drinking water for 3 days.

After the surgery, the clinical condition of every single animal was scored for 7 days to ensure their full recovery. Further experiments were conducted four weeks after the injections to allow the retrograde transport of the beads up the axons to the cell bodies of the neurons projecting onto neurons within the LA. To induce fear-related cFos expression, mice underwent auditory cued FC.

2.9 Statistical analysis

All statistical tests were performed in GraphPad Prism 8. First, measured cFos levels were normalized to the averaged cFos expression of the set of four mice that were processed at the same time to reduce variability arising from methodical causes. Normality was assessed for each experimental group using Shapiro-wilk normality test. If a data set passed normality, outliers were determined with the ROUT test. For non-parametric data sets, the interquartile

range method, defining an outlier as 1.5 x interquartile range from the upper and the lower quartile, was applied. After removing significant outliers, the data was again tested for normal distribution followed by two-way ANOVA with Tukey's post-hoc multiple comparisons. Results are plotted as percentage of the WT control. All data are presented mean ± SEM. Significance thresholds are defined as * $p < 0.05$, ** $p < 0.01$ and *** $p < 0.001$.

2.10 Contributions

All experiments were performed under supervision of Heba Ali (H.A.) and Dilja Krueger-Burg (D.K.-B). H.A. and D.K.-B. conceived the study based on the results of previous experiments conducted by H.A. and Olga Babaev (O.B.). Due to the Covid-19 lockdown and the resulting limitations with both access to the lab and animal license approval, H.A. conducted the behavior and perfusions for all the animals in the general and cell-type-specific cFos data sets and developed the macros for image processing as well as the quantification strategy in Imaris. Further, H.A. performed the immunohistochemistry, imaging and analysis for the first n = 4 of amygdala slices. To ensure consistency, H.A. took over the image processing for all subsequent sets of mice that were included in the amygdala experiment. I conducted immunohistochemistry, imaging and the statistical analysis for the remaining n = 12. All steps of data acquisition, image processing and analysis within the mPFC, the AuC and the PAG were performed by me. To establish the retrograde tracing experiment, I performed stereotactic surgeries under supervision of H.A., conducted the behavioral assessment and perfusions, as well as all steps of image acquisition. Parts of the data presented in this work are published in the PhD thesis of H.A. with the title "Role of Neuroligin2 and its interacting inhibitory synapse organizers in the circuits of fear and anxiety".

3 Results

3.1 Nlgn2 deletion results in a strong deficit in fear recall of auditory cued memories

In previous experiments in our laboratory, it was demonstrated by O.B. and H.A. that Nlgn2 KO mice have a strong impairment in auditory cued FC which is not due to deficits in hearing or motor ability (unpublished data). These results were confirmed by H.A. and myself in the context of the present study, and in particular in the cohort of mice that were subsequently used for cFos induction assay (Figure 6).

First, baseline freezing on both training and testing day were plotted and analyzed to serve as controls. In line with their anxiety phenotype, Nlgn2 KO mice showed significantly increased freezing levels compared to their WT littermates when being placed in the novel environment (conditioning chamber) on training day. This phenotype is reflected by a main effect of the genotype ($p < 0.0001$) detected by two-way ANOVA (Figure 6 B). To rule out context generalization, the tone was presented in a different context on testing and training day, respectively, and baseline freezing was plotted on testing day (Figure 6 C). Both Nlgn2 KO and WT mice showed increased baseline freezing ($p < 0.01$) when they received paired training beforehand, but baseline freezing was still much lower than conditioned freezing specific to the tone.

When measuring conditioned freezing on testing day (Figure 6 D), WT mice that received paired training showed a strong increase in freezing levels ($p < 0.001$) compared to unconditioned WT mice which did not freeze at all to the tone. In contrast, a similar effect of fear learning could be observed in Nlgn2 KO mice and in direct comparison conditioned Nlgn2 KO mice showed significantly less freezing behavior than WT mice ($p < 0.001$). Further, a highly significant effect of both the genotype ($p < 0.0001$) and FC training ($p < 0.0001$) as well as a strong interaction ($p < 0.0001$) were revealed by two-way ANOVA. Taken together, these data show that Nlgn2 deletion causes a strong deficit in cued FC.

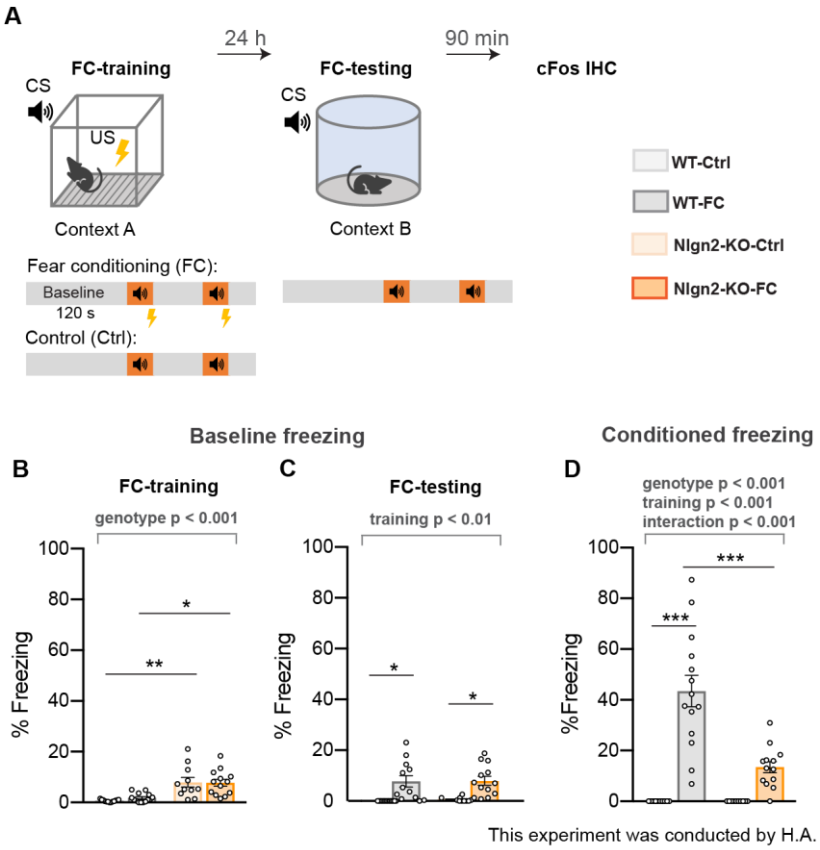

Figure 6: Behavioral phenotype of Nlgn2 KO mice in auditory cued FC. Experimental design of auditory cued FC paradigm. On training day, either two tone-shock sequences or the tone only were presented. On testing day, the tone was presented in absence of the foot shock and freezing levels were measured. CS, conditioned stimulus; US, unconditioned stimulus. **B-C)** Baseline freezing. Two-way ANOVA training day (B): Main effect of genotype: $F(1, 47) = 35.36$, $p < 0.0001$; main effect of training: $F = (1, 47) = 0.1691$, $p = 0.6828$; main effect of interaction: $F(1, 47) = 0.3630$, $p = 0.5497$. Two-way ANOVA testing day (B): Main effect of genotype: $F(1, 45) = 0.0627$, $p = 0.8034$; main effect of training: $F(1, 45) = 28.06$, $p < 0.0001$; main effect of interaction: $F(1, 45) = 0.01838$, $p = 0.8928$. **D)** Conditioned freezing. Two-way ANOVA: Main effect of genotype: $F(1, 45) = 15.62$, $p < 0.0003$; main effect of training: $F(1, 45) = 56.35$, $p < 0.0001$; main effect of interaction $F(1, 45) = 15.62$, $p < 0.0003$. Tukey's post-hoc test: * $p < 0.05$; ** $p < 0.01$ and *** $p < 0.001$. Significant Two-way ANOVA results are marked in grey on top of the graphs. Error bars are presented mean ± SEM. n = 11-14 (B), n = 11-13 (C) and n = 11-14 (D) for each condition.

3.2 Validation of the anti-cFos antibody

For the validation of the guinea pig anti-cFos antibody (catalog# 226 005, Synaptic Systems, Göttingen, Germany) used in this study, brain slices derived from WT mice that were either home caged or exposed to the open field test (OF) before perfusion were stained with the new guinea pig anti-cFos antibody and the rabbit polyclonal anti-cFos antibody (catalog# sc-52, Santa Cruz Biotech, Dallas, Texas, USA). The latter one which was used for cFos

quantifications in previous publications of our group (Babaev et al. 2016; Babaev et al. 2018a) was no longer produced for which reason a new antibody had to be validated prior to the experiments. During the OF test, mice were placed in a novel anxiogenic context. This exposition induces higher expression of neuronal activity marker cFos within the BLA than under home cage conditions. To compare both antibodies, the number of cFos puncta within the LA and the BA was quantified by manually thresholding the confocal images and using "cell counter" plugin in ImageJ for quantification. Although this analysis was preliminary and the number of quantified slices was very low, both antibodies detected a clear increase in cFos expression in both amygdala nuclei under anxiogenic conditions (Figure 7). In direct comparison, the guinea pig anti-cFos antibody apparently labeled more cFos-positive cells than the reference antibody from Santa Cruz. Further, both antibodies clearly labeled cFos expressing nuclei and had low background signal.

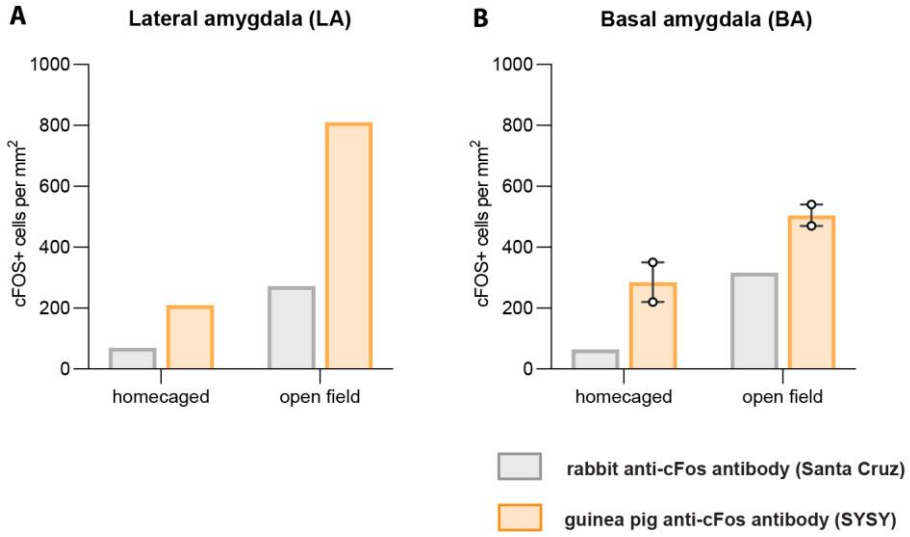

Figure 7: Validation of the guinea pig anti-cFos antibody (SYSY). A-B) cFos quantification showing an increase in cFos expression under anxiogenic conditions that is detected with both antibodies within the LA (A) and the BA (BA). n = 1 for the LA, n = 1 for rabbit anti-cFos antibody (Santa Cruz) and n = 2 for guinea pig anti-cFos antibody (SYSY). Dots represent single data points. Error bars represent mean ± SEM.

3.3 cFos induction assay of the amygdaloid complex

To investigate the neural circuits and the mechanisms underlying the deficit of Nlgn2 KO mice in auditory FC, fear-associated brain regions were immunohistochemically stained and quantified for neuronal activity marker cFos (Sagar et al. 1988). These experiments aimed at identifying the brain region in which the lack of Nlgn2 causes changes that might possibly contribute to the characterized phenotype in cued FC and, thus, at providing a basis for further experiments. Since the existing literature strongly relates cued FC to the LA, we first

focused our work on the amygdaloid complex. Two-way ANOVA results are summarized below (Table 12).

3.3.1 Nlgn2 KO mice show deficits in cFos expression in the LA after fear recall as well as significantly increased cFos levels within the BA

Not surprisingly, the most robust effects of Nlgn2 deletion detected by cFos quantification was observed within the LA (Figure 8 C, G). While WT mice that received paired training showed significantly increased cFos expression compared to WT control animals ($p < 0.001$), a similar effect could not be observed in Nlgn2 KO mice. Further, there was a highly significant effect of FC training ($p < 0.0001$) as well as an interaction between FC and the genotype ($p < 0.05$). Taken together, these data demonstrate that fear conditioned Nlgn2 KO mice show a clear deficit in cFos expression within the LA that is related to FC training.

Within the BA, cFos levels in both Nlgn2 KO and WT mice did not increase in response to fear recall, but paired Nlgn2 KO mice showed significantly higher cFos expression than their WT littermates ($p < 0.01$) (Figure 8 D, G). Two-way ANOVA revealed a main effect of the genotype with the KO mice showing an overall higher activation ($p < 0.001$).

A similar analysis of both the CeL and the CeM did not reveal any significant differences between Nlgn2 KO and WT mice, nor there was an effect of genotype, FC training or an interaction between both factors (Figure 8 E, F).

To rule out that cFos results are falsified by differences in the size of the respective outlined region, I plotted the measured areas for each region and importantly, none of these controls showed significant differences (Figure 16 A-D).

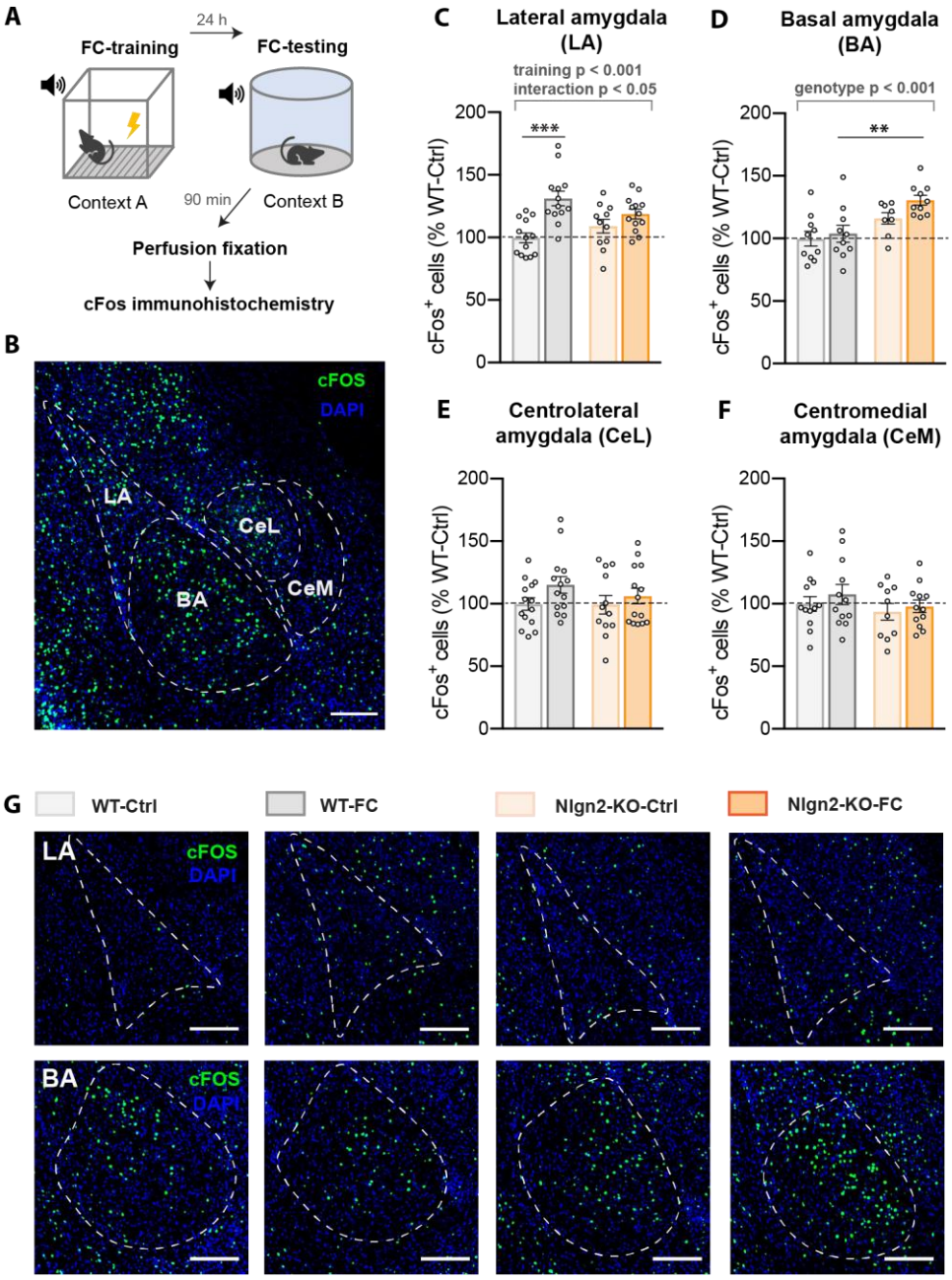

Figure 8: Fear-induced cFos expression in the amygdaloid complex. A) Experimental design of fear-induced cFos induction assay. Mice underwent auditory cued FC paradigm, were perfused 90 min after fear recall and coronal brain slices containing the amygdala were quantified for cFos expression. **B)** Low magnification overview image of the amygdala. The regions included in the analysis are schematically outlined. Scale bar = 200 µm. **C-F)** Normalized cFos expression within the LA (C), BA (D), CeL (E) and CeM (F) of fear conditioned WT and Nlgn2 KO mice as well as unconditioned controls of both genotypes. Expression of neuronal activity marker cFos was induced by exposure to the CS on testing day. Tukey's post-hoc test: * $p < 0.05$; ** $p < 0.01$. Significant two-way ANOVA results are marked in grey on top of the graphs and all two-way ANOVA comparisons are summarized in Table 12. n = 14 (C, E), n = 8 (D), n = 12 (F) for each condition. Dots represent single data points. Error bars represent mean ± SEM. **G)** Representative images illustrating the phenotypes in the LA and the BA. Scale bar = 200 µm.

3.4 Cell-type-specific cFos induction assay of the amygdala

In addition, we sought to shed a light on how the function of local GABAergic neuronal populations within the amygdala might be perturbed by Nlgn2 deletion. To dissect the distinct cell types, brain slices were co-labeled for neuronal activity marker cFos and GABAergic cellular markers and analyzed for colocalization. The antibodies used for this experiment were validated and optimized for their concentration prior to experiments either by me and H.A. or by O.B.. Two-way ANOVA results are summarized below (Table 12).

3.4.1 Nlgn2 deletion causes a deviant activation pattern of VIP+ neurons within the LA

Co-localization analysis of PV+ neurons with cFos in LA did not reveal changes when directly comparing conditioned Nlgn2 KO and WT mice (Figure 9 D), but there was a significant effect of the genotype ($p = 0.0464$), with PV+ neurons showing an overall higher activation in Nlgn2 KO mice. Further, there was a trend towards downregulation of PV+ neurons in mice of both genotypes that received paired FC training.

Unexpectedly, the most robust effect was observed for VIP+ neurons in the LA (Figure 9 F). While there was a trend towards a decrease in activation in WT mice in response to FC, the opposite tendency occurred in Nlgn2 KO mice. Two-way ANOVA detected a highly significant interaction between the genotype and FC ($p = 0.0069$), but no main effects of the genotype or FC training. Last, similar analysis for SOM+ neurons within the LA did not detect any significant effects (Figure 9 E).

To rule out that the results might be biased by differences in the number of detected cells, I also plotted the total number cells per animal and brain region (Figure 9 G-I) and importantly, none of these controls showed significant effects.

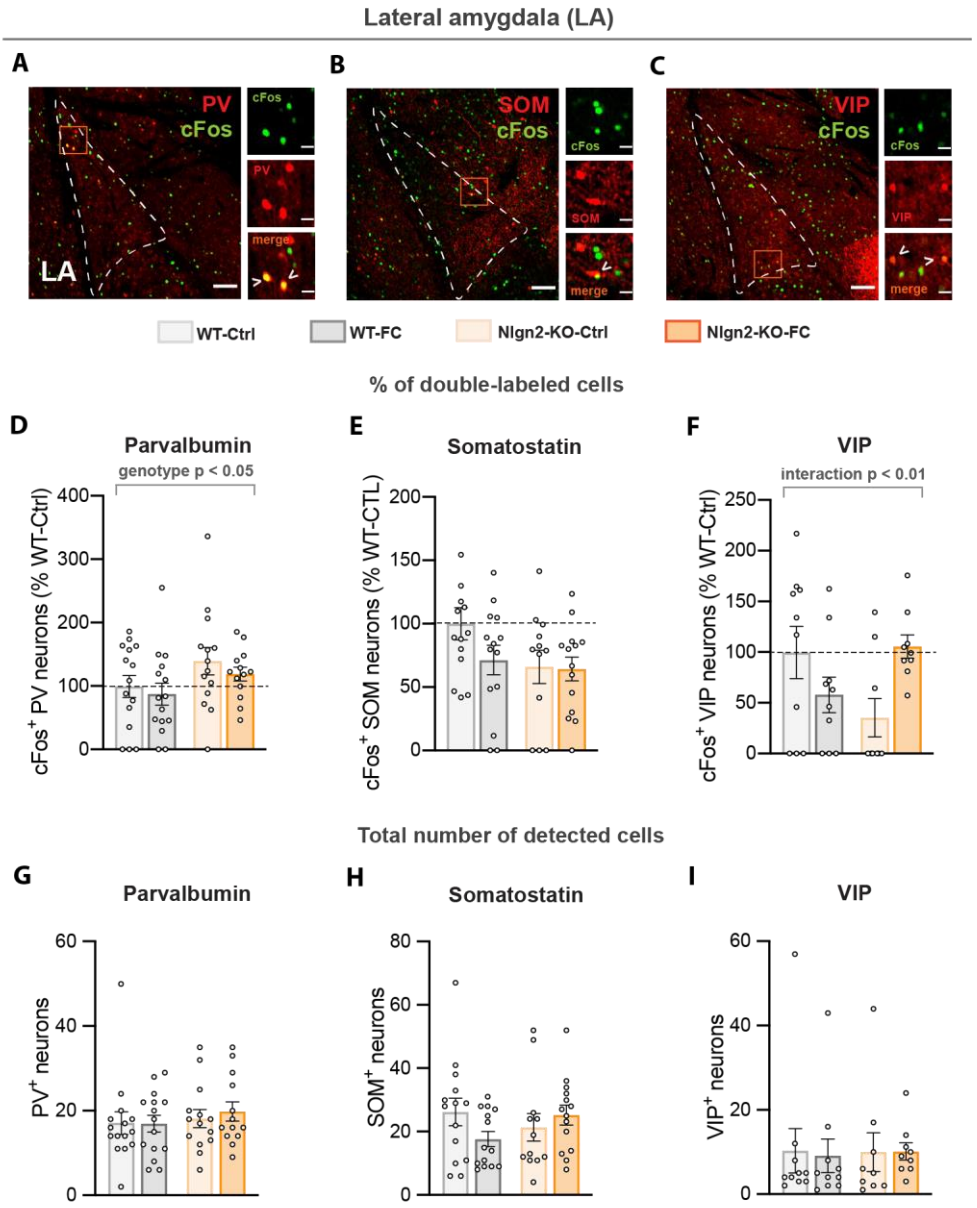

Figure 9: Activation pattern of LA inhibitory neurons. A-C) Representative images for co-labeling of inhibitory neuronal markers with cFos within the LA. PV (A), SOM (B) and VIP (C). Scale bar = 100 µm for overviews, scale bar = 20 µm for high magnification images. Arrow heads mark double-labeled cells. **D-F)** Quantification of the percentage of cells that is double-labeled out of the total number of detected cells expressing the respective cellular marker. PV (D), SOM (E) and VIP (F). Expression of neuronal activity marker cFos was induced by exposure to the CS on testing day. Tukey's post-hoc test: * $p < 0.05$; ** $p < 0.01$. Significant two-way ANOVA results are marked in grey on top of the graphs and all two-way ANOVA comparisons are summarized in Table 12. n = 14 (D, E), n = 8-10 (F) for each condition. **G-I)** Quantification of the total number of detected neurons per animal within the LA that express PV (G), SOM (H) and VIP (I). Since this quantification serves as control, every animal that was included in the cFos plots is also reflected in the number of cells. No significant effects occurred. $F < 1$ for all ANOVA comparisons. Dots represent single data points. Error bars represent mean ± SEM.

3.4.2 No changes were observed in the BA inhibitory network of Nlgn2 KO mice.

A similar cell type-specific cFos analysis of the inhibitory network in the BA did not reveal any significant effects. However, PV+ neurons showed a comparable trend of downregulation in response to FC (Figure 10 D) as it became apparent within the LA, and for SOM+ neurons, there was a trend towards increased activation caused by FC training (Figure 10 E). There was no effect observed in VIP+ neurons (Figure 10 F). I further plotted the total number of detected cells per animal and again, none of these controls became significant.

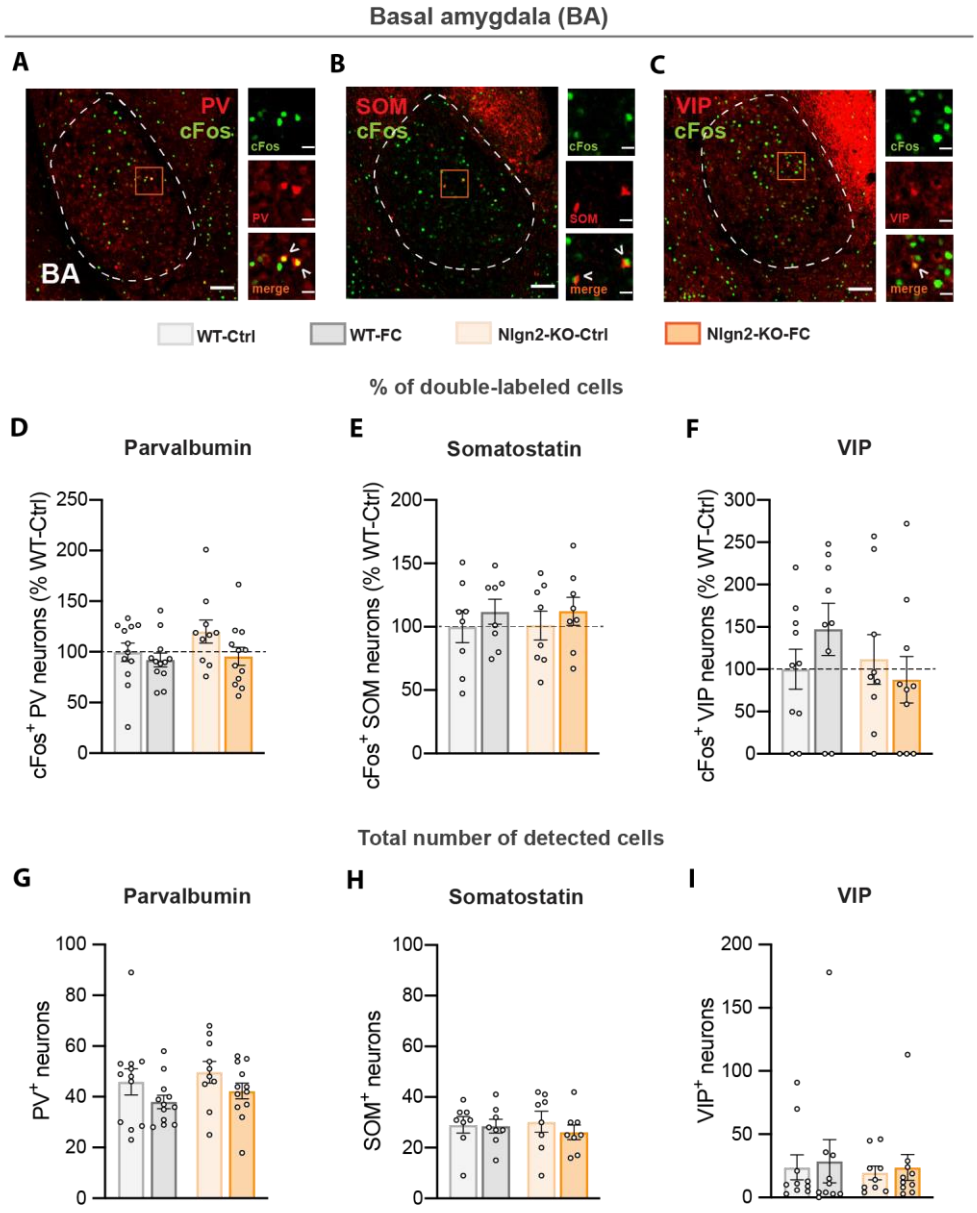

Figure 10: Activation pattern of BA inhibitory neurons. A-C) Representative images for co-labeling of inhibitory neuronal markers with cFos within the BA. PV (A), SOM (B) and VIP (C). Scale bar = 100 µm for overviews, scale bar = 20 µm for high magnification images. Arrow heads mark double-labeled cells.

D-F) Quantification of the percentage of cells that is double-labeled out of the total number of detected cells expressing the respective cellular marker. PV (D), SOM (E) and VIP (F). Expression of neuronal activity marker cFos was induced by exposure to the CS on testing day. Tukey's post-hoc test: * $p < 0.05$; ** $p < 0.01$. Significant two-way ANOVA results are marked in grey on top of the graphs and all two-way ANOVA comparisons are summarized in Table 12. $n = 14$ (C, E), $n = 8$ (D), $n = 12$ (F) for each condition. **G-I)** Quantification of the total number of detected neurons per animal within the LA that express PV (G), SOM (H) and VIP (I). No significant effects were observed. Dots represent single data points. Error bars represent mean ± SEM.

3.4.3 Nlgn2 KO mice do not show an aberrant activation pattern of inhibitory neurons in CeL

Cell-specific cFos quantification of CeL did not reveal any significant shifts in activation between fear conditioned WT and Nlgn2 KO mice either for PKC-δ+ (Figure 11 C) or for SOM+ (Figure 11 D) neurons. Nevertheless, there is a very weak trend towards SOM+ neurons being less activated and PKC-δ+ being more activated in Nlgn2 KO mice than in their WT littermates.

A similar cFos analysis for SOM+ neurons within the CeM (Figure 11 E) identified a significant effect of the genotype ($p = 0.0239$), but no effect of FC training and no interaction. Further, post-hoc analysis did not reveal any significant differences. However, the role of CeM SOM+ neurons in the amygdala fear-processing network remains completely unexplored. Again, the quantification of the total number of detected cells per anatomical region did not reveal any significant effects neither of the genotype, nor of FC training on the number of counted cells in the CeA (Figure 11 F-H).

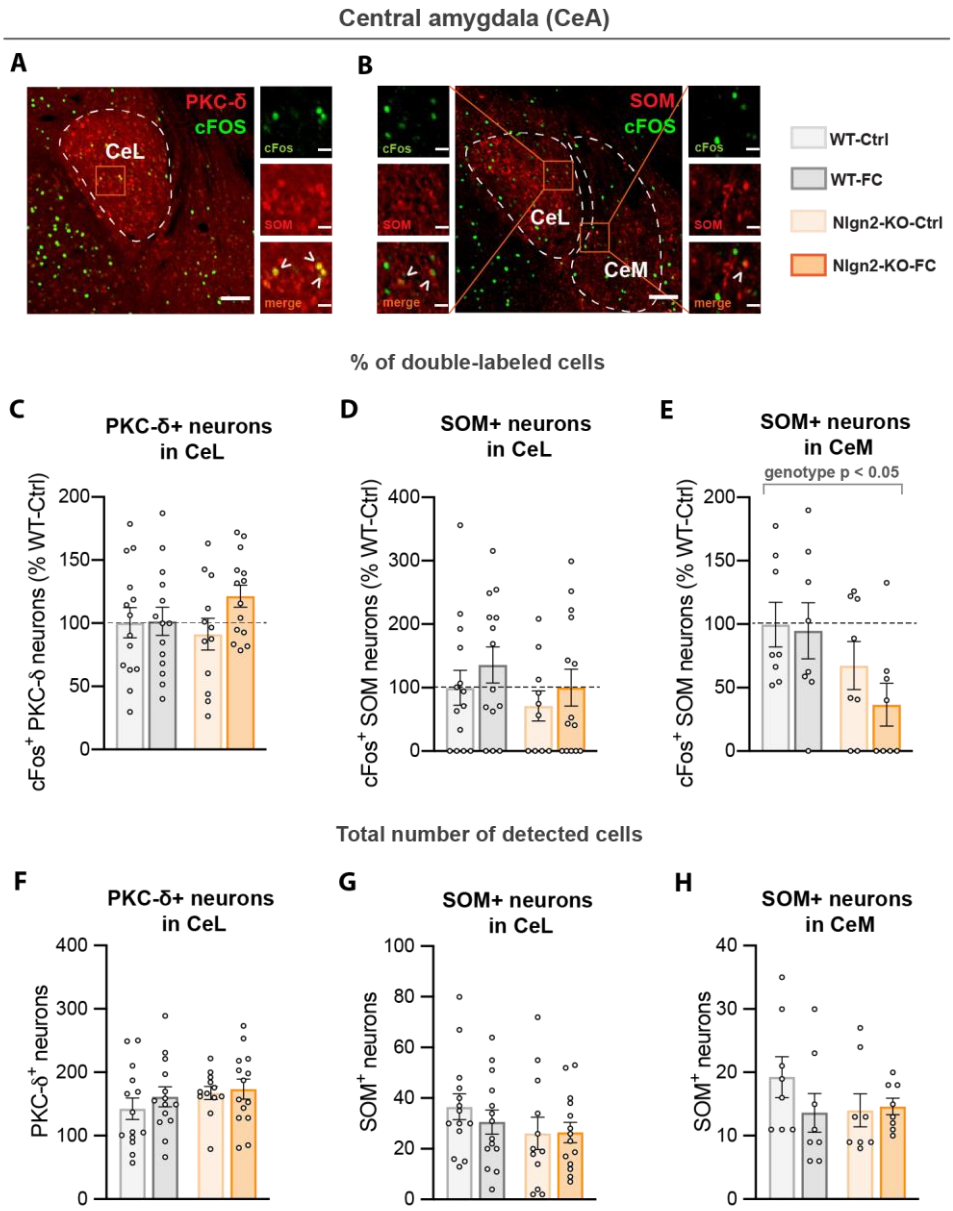

Figure 11: cFos assay of SOM+ and PKC-δ+ neurons in CeA. A-B) Representative images for co-labeling of inhibitory neuronal markers with cFos within the CeA. PKC-δ (A) and SOM (B). Scale bar = 100 µm for overviews, scale bar = 20 µm for high magnification images. Arrow heads mark double-labeled cells. **C-E)** Quantification of the percentage of cells that is double-labeled out of the total number of detected cells expressing the respective cellular marker. PKC-δ (C), SOM in CeL (D) and SOM in CeM (E). Expression of neuronal activity marker cFos was induced by exposure to the CS on testing day. Tukey's post-hoc test: * $p < 0.05$; ** $p < 0.01$. Significant two-way ANOVA results are marked in grey on top of the graphs and all two-way ANOVA comparisons are summarized in Table 12. n = 14 (C, D), n = 8 (E) for each condition. Dots represent single data points. Error bars represent mean ± SEM. **F-H)** Quantification of the total number of detected neurons per animal within the CeA that express PKC-δ (F) and SOM (G, H). Since this quantification serves as control, every animal that was included in the cFos plots is also reflected in the number of cells. No significant effects occurred. $F < 1$ for all ANOVA comparisons.

Table 12: Two-way ANOVA comparison results of cFos induction assay of the amygdala.

Two-way ANOVA comparisons						
Figure	**Main effect genotype F-value**	**Main effect genotype p-value**	**Main effect FC training F-value**	**Main effect FC training p-value**	**Main effect interaction F-value**	**Main effect interaction p-value**
8 C	F (1, 46) = 0.1163	0.7346	F (1, 46) = 18.45	<0.0001	F (1, 46) = 5.176	0.0276
8 D	F (1, 34) = 14.8	0.0005	F (1, 34) = 2.767	0.1054	F (1, 34) = 0.8671	0.3583
8 E	F (1, 50) = 0.5663	0.4553	F (1, 50) = 3.145	0.0822	F (1, 50) = 0.4508	0.5050
8 F	F (1, 42) = 2.634	0.1119	F (1, 42) = 1.844	0.1816	F (1, 42) = 0.1262	0.7242
9 D	F (1, 27) = 3.106	0.0893	F (1, 27) = 4.215	0.0499	F (1, 27) = 9.879	0.0040
9 E	F (1, 34) = 1.009	0.3223	F (1, 34) = 0.3289	0.5701	F (1, 34) = 1.616	0.2123
9 F	F (1, 52) = 4.122	0.0475	F (1, 52) = 0.7709	0.3840	F (1, 52) = 0.1152	0.7357
10 D	F (1, 42) = 1.752	0.1927	F (1, 42) = 3.092	0.0860	F (1, 42) = 0.8790	0.3538
10 E	F (1, 50) = 2.991	0.0899	F (1, 50) = 1.646	0.2054	F (1, 50) = 1.299	0.2598
10 F	F (1, 28) = 0.007894	0.9298	F (1, 28) = 1.050	0.3143	F (1, 28) = 0.000316	0.9859
11 C	F (1, 48) = 0.07573	0.7844	F (1, 48) = 0.02380	0.8781	F (1, 48) = 0.7285	0.3976
11 D	F (1, 28) = 5.691	0.0241	F (1, 28) = 0.8706	0.3588	F (1, 28) = 0.4786	0.4948
11 E	F (1, 50) = 0.2238	0.6382	F (1, 50) = 1.921	0.1719	F (1, 50) = 1.638	0.2065

3.5 cFos induction assay of fear-related upstream regions

Given that we detected significant changes in the activation pattern of the LA in Nlgn2 KO mice, the main question that arose was whether these alterations mechanistically originate there or if they only reach the amygdala through projections from its upstream regions. For this reason, I further conducted a cFos induction assay of the AuC and the mPFC. Two-way ANOVA results are summarized below (Table 13).

3.5.1 Nlgn2 KO mice show pronounced changes in cFos expression within the primary auditory cortex (Au1)

To address the question whether the AuC might contribute to the Nlgn2 KO phenotype in FC, I performed a cFos analysis on the distinct subregions of the AuC (Figure 12 A) according to the experiments conducted within the amygdala. To this end, I used the animals that were initially intended for the tracing experiment, since their behavioral phenotype in fear recall was not altered by the stereotactic surgeries (Figure 19 C). An additional n of 3 animals per condition was added to complete the data set.

Quantification of neuronal activity marker cFos revealed a deficit in cFos expression in conditioned Nlgn2 KO mice which was particularly prominent within the Au1. First, there was a strong interaction between FC training and the genotype ($p < 0.01$). WT mice that received paired training showed a significant increase of cFos expression compared to their naive littermates after presentation of the CS ($p < 0.05$). In sharp contrast, conditioned Nlgn2 KO mice even showed slightly reduced cFos levels in comparison to their baseline expression in unconditioned animals (Figure 12 B). Further, conditioned WT mice had significantly increased cFos expression in direct comparison to conditioned Nlgn2 KO mice ($p < 0.05$). No main effects either of the genotype or of FC training were observed and the measured area of Au1 per animal did not differ between Nlgn2 KO and WT mice (Figure 16 H). A similar cFos analysis of the ventral part of the secondary AuC (AuV) did not reveal any effects (Figure 12 C). Comparable to the changes observed in the Au1, there was a significant interaction ($p < 0.05$) within the dorsal part of the secondary AuC (AuD), but no effect of the genotype or FC training (Figure 12 D).

As the general cFos assay revealed substantial changes in the activation pattern of the Au1, this finding was further pursued with an interneuron-specific cFos quantification. Although the number of animals included in the analysis was very small, a significant effect of FC training ($p < 0.05$) could be observed in VIP+ neurons. VIP+ neurons in both Nlgn2 KO and WT mice showed an increase in cFos expression in response to presentation of the CS on testing day, but there was a trend towards higher activation in WT mice (Figure 13 A). Interestingly, the total number of detected VIP+ neurons was reduced in Nlgn2 KO mice that received paired FC training in comparison with conditioned WT mice and this trend was very close to significance ($p = 0.0599$). Further, this effect was also reflected in a main effect of interaction between FC and the genotype which was almost significant ($p = 0.0514$) (Figure 13 F). There were no significant effects either in PV+ (Figure 13 B) or in SOM+

(Figure 13 C) and the total number of counted PV+ cells was not altered in Nlgn2 KO mice compared to their WT littermates (Figure 13 G).

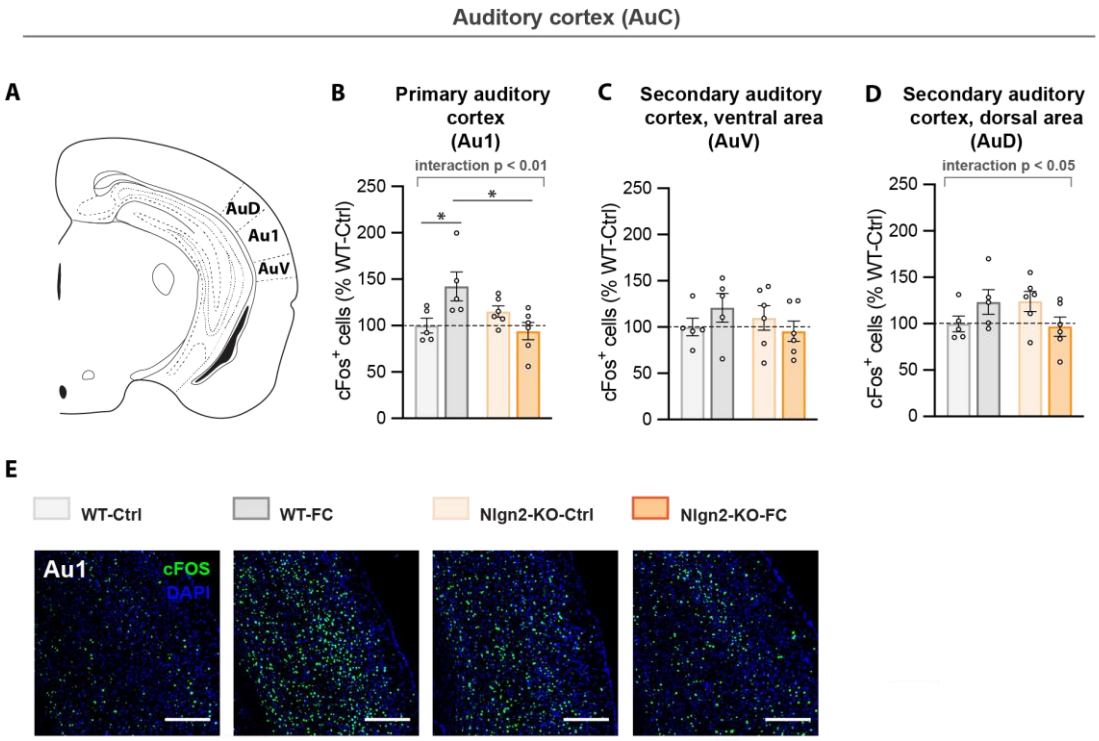

Figure 12: Fear induced cFos expression of the AuC. A) Schematic overview of the AuC illustrating the regions that were included in the analysis. **B-D)** Quantification of cFos+ nuclei in Au1 (B), AuV (C) and AuD (D). n = 5-6 for each condition. Tukey's post-hoc test: * $p < 0.05$. Significant two-way ANOVA results are marked in grey on top of the graphs and all two-way ANOVA comparisons are summarized in Table 13. Dots represent single data points. Error bars represent mean ± SEM**. E)** Representative images illustrating the phenotypes within Au1 region. Scale bar = 100 µm.

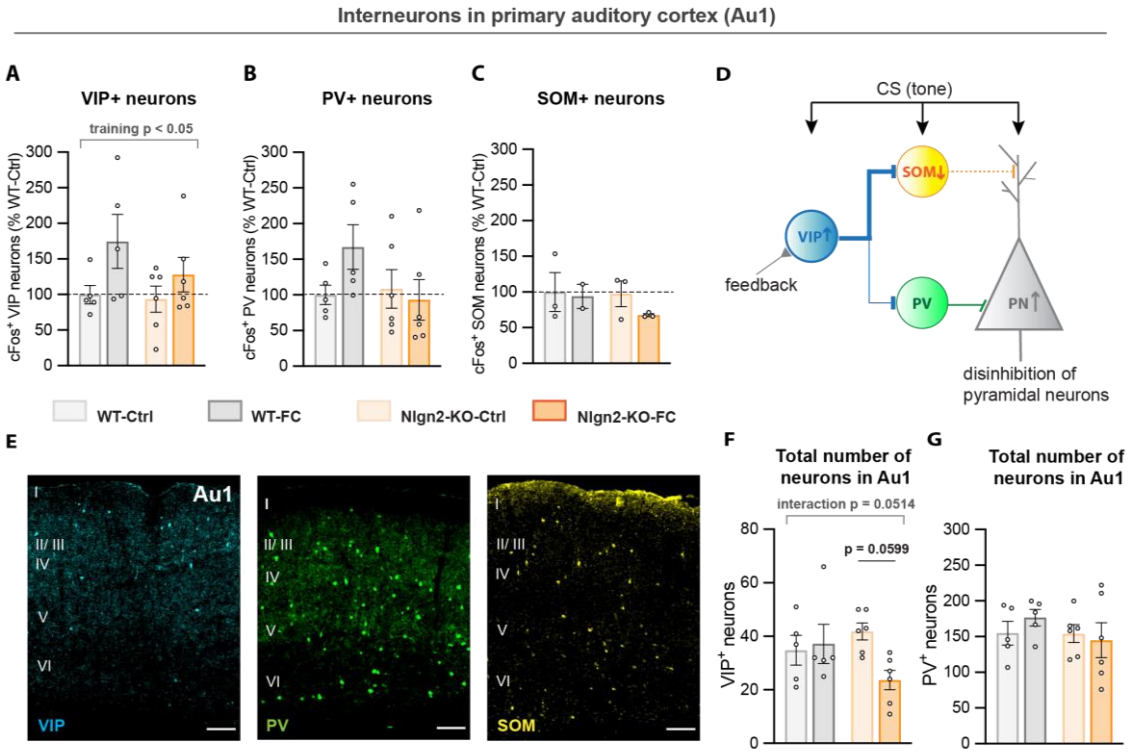

Figure 13: Activation pattern of interneurons in Au1. A-C) Quantification of the percentage of cells double labeled for cFos and cellular markers out of the total number of detected cells within Au1. VIP (A), PV (B) and SOM (C). Expression of neuronal activity marker cFos was induced by exposure to the CS on testing day. Significant two-way ANOVA results are marked in grey on top of the graphs and all two-way ANOVA comparisons are summarized in Table 13. n = 5-6 (A, B) and n = 2-3 (C). **D)** Model on the disinhibitory microcircuit for associative learning. Feedback information reaching VIP+ neurons disinhibits specific subpopulations of glutamatergic projection neurons through inhibition of inhibitory neuronal populations. Created after (Pi et al. 2013) with permission from Springer Nature. **E)** Representative images illustrating the distribution pattern and number of specific interneurons across the AuC. Numbers on the left represent the cortical layers. Scale bar = 100 µm. **F-G)** Quantification of the total number of detected neurons per animal within the Au1 that express VIP (G) and PV (F). Since this quantification serves as control, every animal that was included in the cFos plots is also reflected in the number of cells. Dots represent single data points. Error bars represent mean ± SEM.

3.5.2 Fear-induced cFos expression pattern is changed in PrL, but not in IL area of Nlgn2 KO mice

I further performed a cFos induction assay on the mPFC, an important cortical component of the fear-processing network. Comparable to the effect that was observed in the LA, WT mice showed a significant increase in cFos expression within the PrL when they received paired FC training ($p < 0.01$) (Figure 14 C). In contrast, this effect was not observed in Nlgn2 KO mice. Further, baseline cFos expression was significantly higher in unconditioned Nlgn2 KO mice than in unconditioned WT mice ($p < 0.05$). Two-way ANOVA revealed significant

effects of both the genotype ($p < 0.01$) and FC ($p < 0.001$), but no interaction between both factors. Within the IL, there was a main effect of FC training ($p < 0.05$), but no differences between Nlgn2 KO and WT mice could be observed (Figure 14 D). However, these findings are interesting, but were not further pursued in this study, since they presumably do not explain the deficit in auditory FC observed in Nlgn2 KO mice.

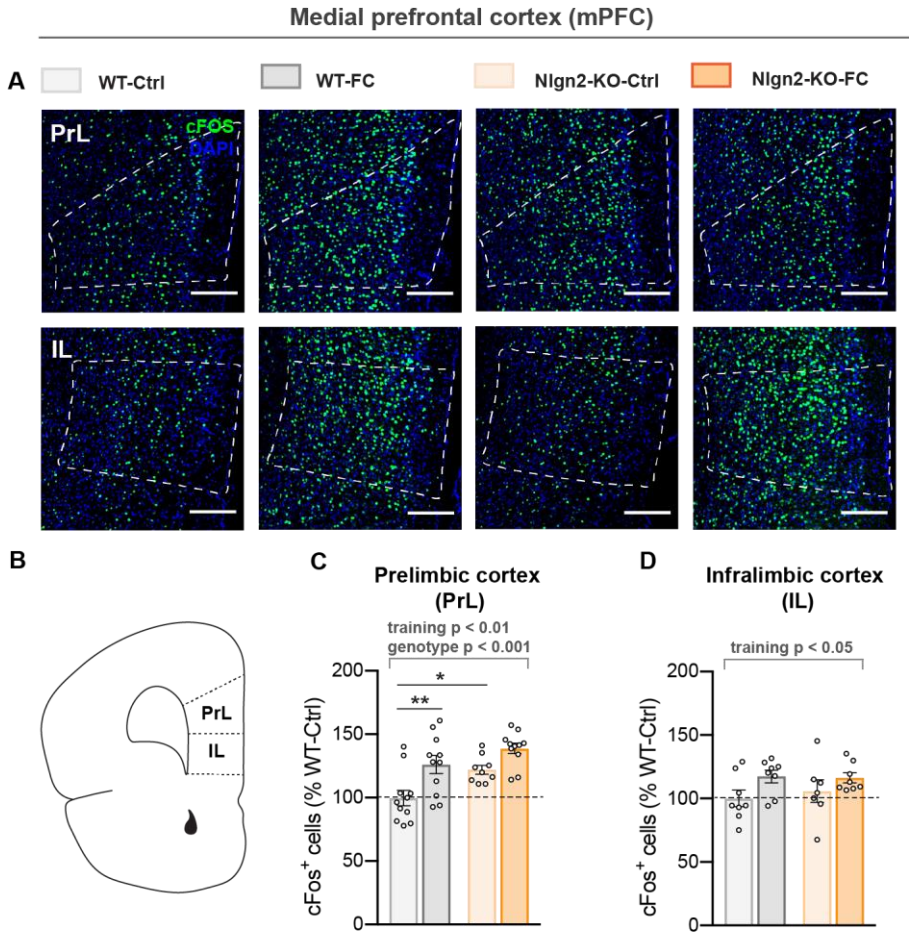

Figure 14: Fear-induced cFos expression of the mPFC. **A)** Representative images illustrating the phenotypes detected by quantification of cFos expression induced by presentation of the CS on testing day. The outlining indicates the regions that were included in the analysis. Scale bar = 200 µm. **B)** Schematic illustration of the regions that were included in the analysis. **C-D)** Quantification of cFos expressing neurons in PrL (C) and IL (D). Tukey's post-hoc test: * $p < 0.05$; ** $p < 0.01$. Significant Two-way ANOVA results are marked in grey on top of the graphs and all Two-way ANOVA comparisons are summarized in Table 13. n = 11-12 (C), n = 8 (D) for each condition. Dots represent single data points. Error bars represent mean ± SEM.

3.6 cFos induction assay of downstream regions

Since we sought to find a downstream correlate for the behavioral phenotype of Nlgn2 KO mice in auditory FC, I also focused my work on the vlPAG, a brainstem region that was shown being critically implicated in the mediation of freezing.

3.6.1 Activation pattern of the vlPAG does not differ in WT and Nlgn2 KO mice

Strikingly, cFos quantification of the vlPAG (Figure 15 B) did not reveal any significant differences between fear conditioned Nlgn2 KO and their WT littermates that might possibly contribute to the robust behavioral phenotype in FC. However, there was a significant main effect of FC training ($p < 0.05$), but neither an effect of the genotype, nor there was an interaction between both factors.

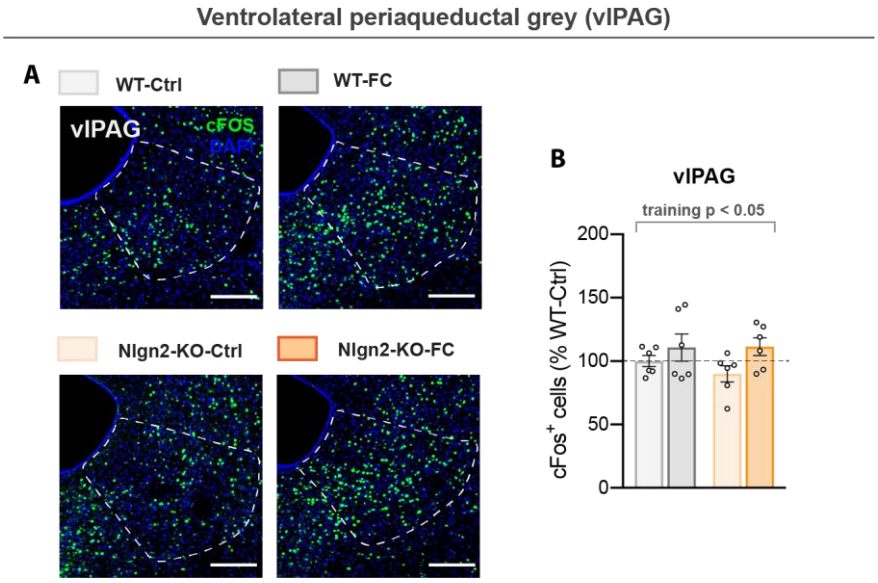

Figure 15: Fear-induced cFos expression in brain stem effector region vlPAG. A) Representative images illustrating the phenotypes detected by quantification of cFos expression induced by presentation of the CS on testing day. The outlining indicates the regions that were included in the analysis. Scale bar = 200 µm. **B)** Quantification of cFos expressing neurons in vlPAG after presentation of the CS on testing day. Significant two-way ANOVA results are marked in grey on top of the graphs and all Two-way ANOVA comparisons are summarized in Table 13. n = 6 for each condition. Dots represent single data points. All bars represent mean ± SEM.

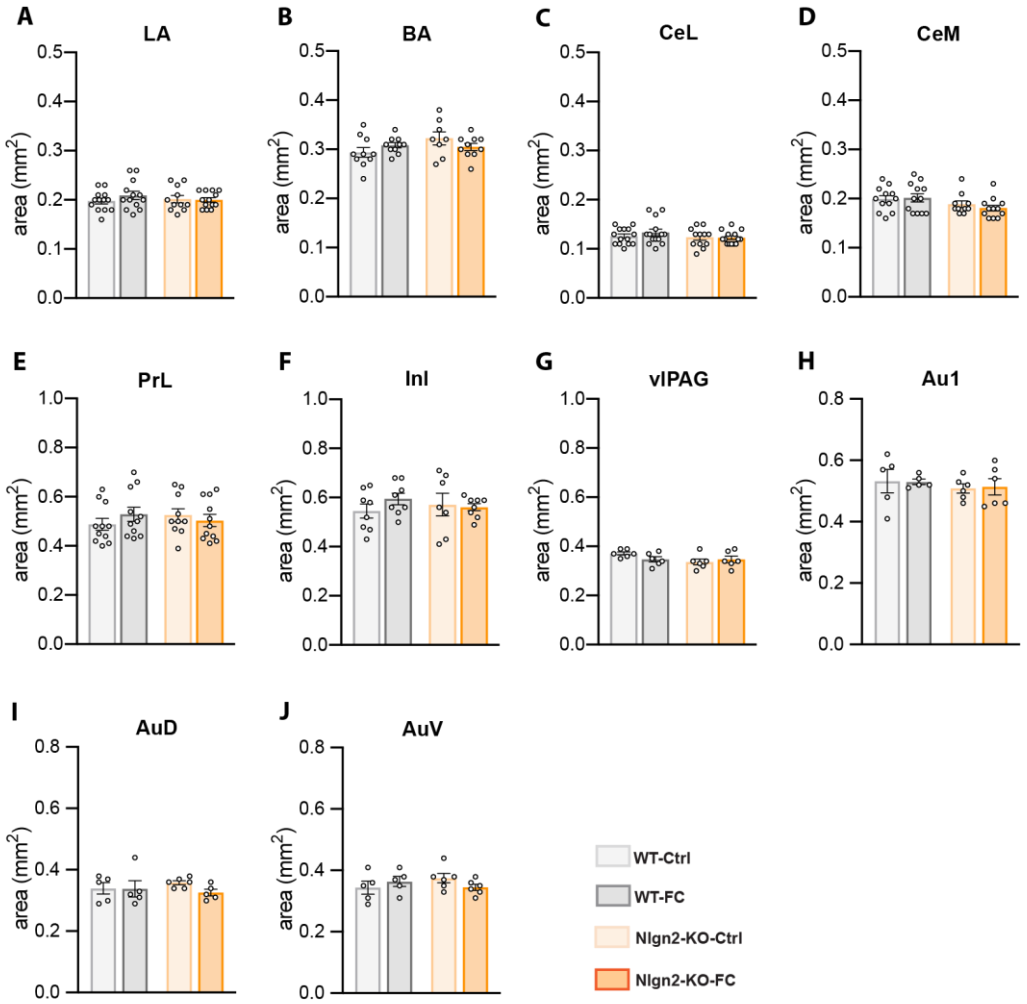

Figure 16: Area controls for quantification of general cFos expression. A-J) Measured area per animal and brain region to verify that the detected changes in cFos levels are not driven by differences in the size of the outlined area. Importantly, none of these controls showed significant effects. Dots represent single data points. All bars represent mean ± SEM.

Table 13: Two-way ANOVA comparisons of the cFos induction assay of the AuC, the mPFC and the vlPAG.

Two-way ANOVA						
Figure	**Main effect genotype F-value**	**Main effect genotype p-value**	**Main effect FC training F-value**	**Main effect FC training p-value**	**Main effect interaction F-value**	**Main effect interaction p-value**
12 B	F (1, 18) = 2.720	0.1164	F (1, 18) = 1.125	0.3028	F (1, 18) = 10.08	0.0052
12 C	F (1, 18) = 0.3756	0.7993	F (1, 18) = 0.067	0.7993	F (1, 18) = 1.948	0.1798
12 D	F (1, 18) = 0.01198	0.9141	F (1, 18) = 0.03258	0.8588	F (1, 18) = 5.442	0.0315
13 A	F (1, 18) = 1.145	0.2987	F (1, 18) = 4.852	0.0409	F (1, 18) = 0.6578	0.4279
13 B	F (1, 18) = 1.516	0.2341	F (1, 18) =0.95	0.3426	F (1, 18) = 2.413	0.1377
13 C	F (1, 7) = 0.5459	0.4840	F (1, 7) = 0.8622	0.3840	F (1, 7) = 0.3819	0.5562
13 F	F (1, 18) = 0.4350	0.5179	F (1, 18) = 2.560	0.1270	F (1, 18) = 4.355	0.0514
13 G	F (1, 18) = 0.8243	0.3759	F (1, 18) = 0.1266	0.7262	F (1, 18) = 0.7606	0.3946
14 C	F (1, 38) = 9.781	0.0034	F (1, 38) = 14.92	0.0004	F (1, 38) = 0.7314	0.3978
14 D	F (1, 27) = 0.1407	0.7105	F (1, 27) = 5.141	0.0316	F (1, 27) = 0.3145	0.5795
15 B	F (1, 20) = 0.3888	0.5400	F (1, 20) = 4.536	0.0458	F (1, 20) = 0.5066	0.4848

3.7 Validation of Cre driver mouse lines for PV, SOM and VIP

In preparation for future experiments of the project, I validated Cre driver mouse lines for PV, SOM and VIP. Cre driver mice were obtained by crossing PV-, SOM- and VIP-Cre animals (Hippenmeyer et al. 2005; Taniguchi et al. 2011) with the CAG-CAT-EGFP line (Nakamura et al. 2006) to allow the Cre-dependent expression of EGFP in the respective cell types. Co-labeling brain slices containing the amygdala obtained from those mouse lines for EGFP and the respective cellular markers further allowed a direct comparison between both staining patterns and the overall number of labeled cells. Hence, the labeling of the Cre driver lines further served as controls for the specificity of the antibodies used for the cellular cFos induction assay.

First, I confirmed that EGFP is exclusively expressed in the respective cell type and that the CAG-CAT-EGFP construct did not spread across the genome. To this end, brain slices containing the amygdala derived from EGFP x Cre double knock-in (KI), as well as Cre only and EGFP only KI mice were stained with an anti-GFP antibody. As illustrated below for the three mouse lines (Figure 17 A-C), EGFP was exclusively expressed in the double KI animals. Second, I used naive slices to validate the endogenous EGFP signal of the cells, since a strong fluorescent signal is required to identify the respective cell types during in vivo or electrophysiological approaches. Apart from the SOM-Cre driver line in which the endogenous EGFP signal was strong (Figure 17 D), the EGFP expression of the other mouse lines was very weak, and I had to use very high laser intensities to visualize the EGFP signal. For this reason, I decided not to image the endogenous EGFP signal of both the VIP- and the PV-Cre driver line.

Further, I co-labeled brain tissue obtained from a SOM-Cre driver animal with an anti-GFP antibody and with the anti-SOM antibody which was used for the cFos assay. Every cell that was labeled by the anti-SOM antibody was also immunoreactive for GFP, but the SOM antibody labeled less cells then the GFP antibody (Figure 18 A). Particularly within the CeL, there is a highly interconnected network of SOM+ fibers causing very dense background signal which was present in both stainings (Figure 18 B).

For the PV-Cre driver line, I calculated a ratio of PV-EGFP-double-labeled neurons out of the total number of EGFP+ neurons, which was about 16.77% within the LA and 40.02% within the BA (Figure 18 C). Importantly, all cells labeled by the anti-PV antibody were also immunoreactive for GFP, supporting the notion that the antibody exclusively labels neurons that contain PV. The finding that there are double-labeled cells in both the SOM- and the PV-Cre driver is relevant, since it confirms that despite the Cre KI the respective neuropeptides are still expressed in the interneurons.

Unfortunately, the VIP staining did not work for technical reasons at the time I validated the VIP-Cre driver mice, prohibiting a direct comparison of the anti-VIP antibody with the EGFP expression pattern in VIP-Cre driver mice.

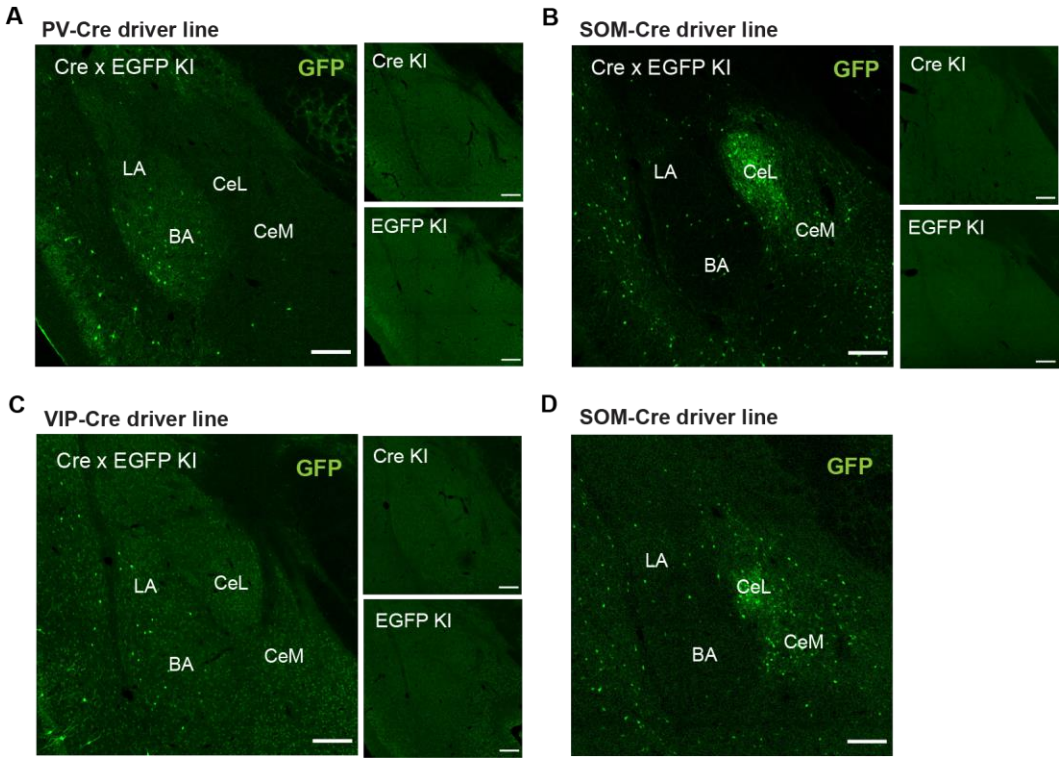

Figure 17: Validation of Cre driver mouse lines for PV, SOM and VIP. A-C) Low magnification overviews of the amygdala demonstrating that EGFP is exclusively expressed in Cre x EGFP double KI animals. EGFP expressing cells are labeled with an anti-GFP antibody. Scale bar = 200 μm. **D)** Endogenous EGFP signal of the SOM-Cre driver line. Scale bar = 200 μm.

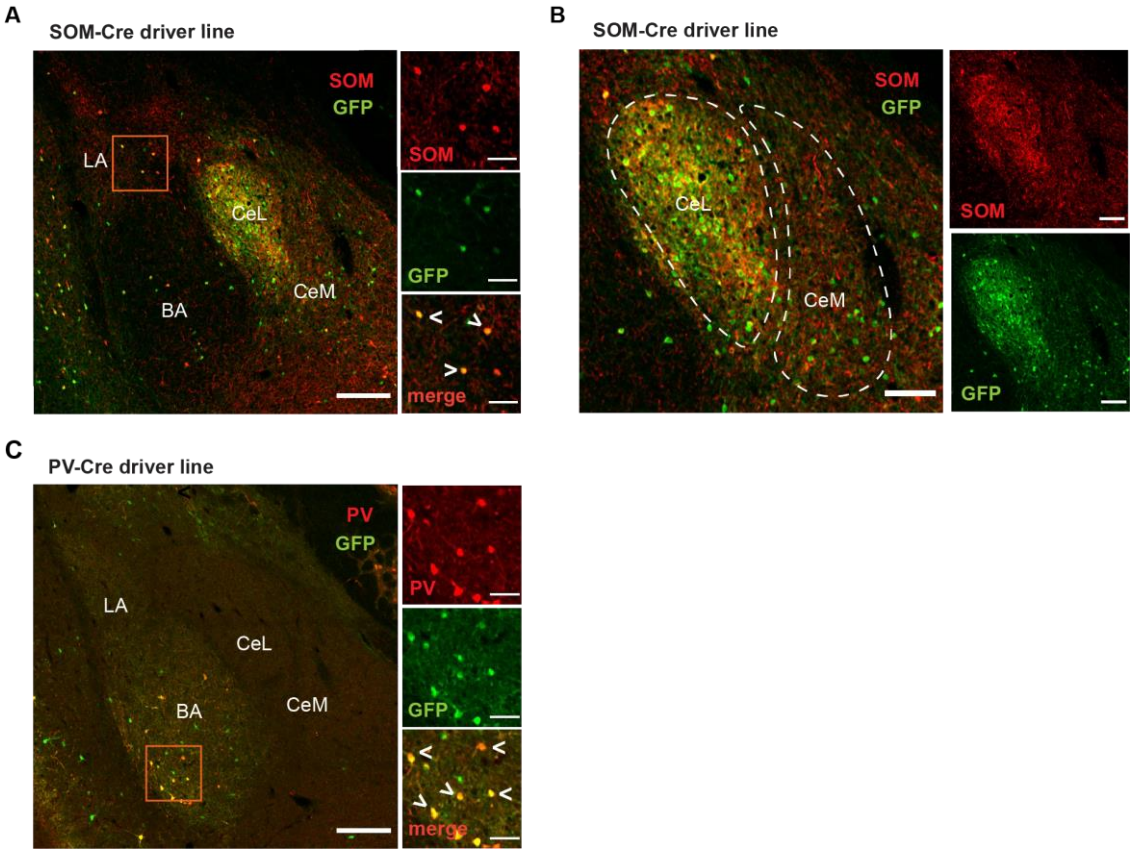

Figure 18: Co-labeling of EGFP+ neurons with the anti-PV and the anti-SOM antibodies used for the cell-specific cFos induction assay. A) Representative overview of the amygdala labeled for SOM and GFP. The tissue was obtained from a SOM-Cre driver animal. **B)** Magnified overview of the CeA labeled for SOM and GFP. Scale bar, 100 µm. **C)** Overview of the amygdala labeled for PV and GFP. The tissue was obtained from a PV-Cre driver animal. Scale bar = 200 µm for overviews and 50 µm for high magnification images. Arrow heads mark double-labeled cells.

3.8 Retrograde tracing of projections to the LA

According to the results of the previous cFos analysis, the LA is among the most likely regions to contribute to the Nlgn2 KO phenotype in FC. However, we could not rule out that the mechanistic changes caused by the lack of Nlgn2 might possibly originate somewhere upstream from the amygdaloid complex and that the changes detected within the LA simply reflect alterations reaching the amygdala from somewhere else. For this reason, I aimed to stereotactically deliver red RetroBeads™ into the LA (Figure 20). Combining retrograde labeling with cFos induction assay facilitates a quantitative assessment of the activation pattern of the projections mentioned above.

First, I performed surgeries and the behavioral assessment on a pilot cohort of 12 animals to rule out that the surgeries interfere with the behavioral phenotype. WT mice that received

surgeries showed higher baseline freezing on training day than naive WT mice did in previous experiments, which could be due to fear generalization induced by the surgeries (Figure 19 A). So far, this effect appears to obscure the innate anxiety behavior of Nlgn2 KO mice, but the sample size was very small and more animals would be required to see whether these few animals are representative. In contrast, the surgeries did not seem to have any major consequences neither on the baseline freezing on testing day nor on conditioned freezing to the CS (Figure 19 B-C).

Second, I aimed at confirming the correct placement of the RetroBeads™ injection within the LA, as well as their expression across the AuC. Given that the LA with a size of about 0.2 mm^2 (Figure 16 A) is a very small anatomical structure which is located very deep within the brain, this experiment was of particularly challenging technical nature. Technical obstacles that arose included backflow of the beads though the injection channel and a lack of precision in hitting the target coordinates (Figure 20 B). Although I chose different coordinates and injection volumes (50 nl, 75 nl and 100 nl), it was not possible to sufficiently establish this complex and important experiment within the remaining amount of time I spent in the lab for my dissertation.

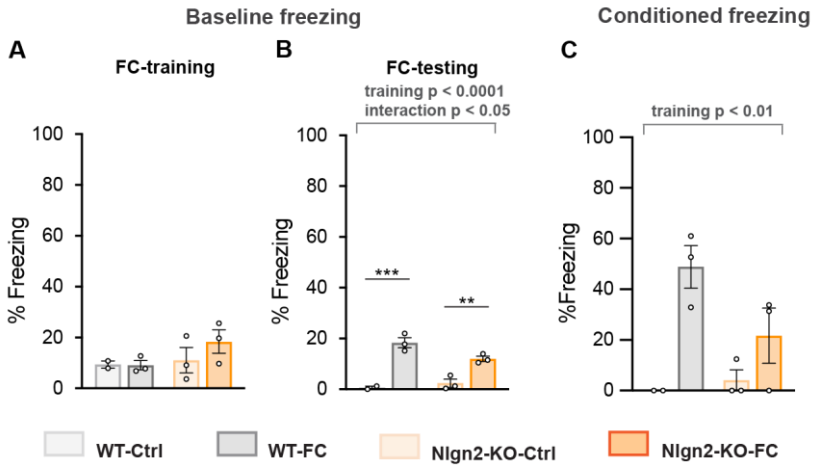

Figure 19: Behavioral assessment of mice that received stereotactic surgeries. A-B) Baseline freezing. Two-way ANOVA training day (B): Main effect of genotype: F (1, 7) = 1.864, p = 0.2144; main effect of training: F = (1, 7) = 0.7513, p = 0.4148; main effect of interaction: F (1, 7) = 0.8534, p = 0.3863. Two-way ANOVA testing day (B): Main effect of genotype: F (1, 7) = 2.111, p = 0.1896; main effect of training: F (1, 7) = 77.16, p < 0.0001; main effect of interaction: F (1, 7) = 0.679, p = 0.0362. **C)** Conditioned freezing. Two-way ANOVA: Main effect of genotype: F (1, 7) = 2.010, p = 0.1992; main effect of training: F (1, 7) = 16.72, p = 0.0046; main effect of interaction F (1, 7) = 3.718, p = 0.0952. Tukey's post-hoc test: * p < 0.05; ** p < 0.01 and *** p < 0.001. Significant two-way ANOVA results are marked in grey on top of the graphs. Error bars are presented mean ± SEM. n = 2-3 for each condition.

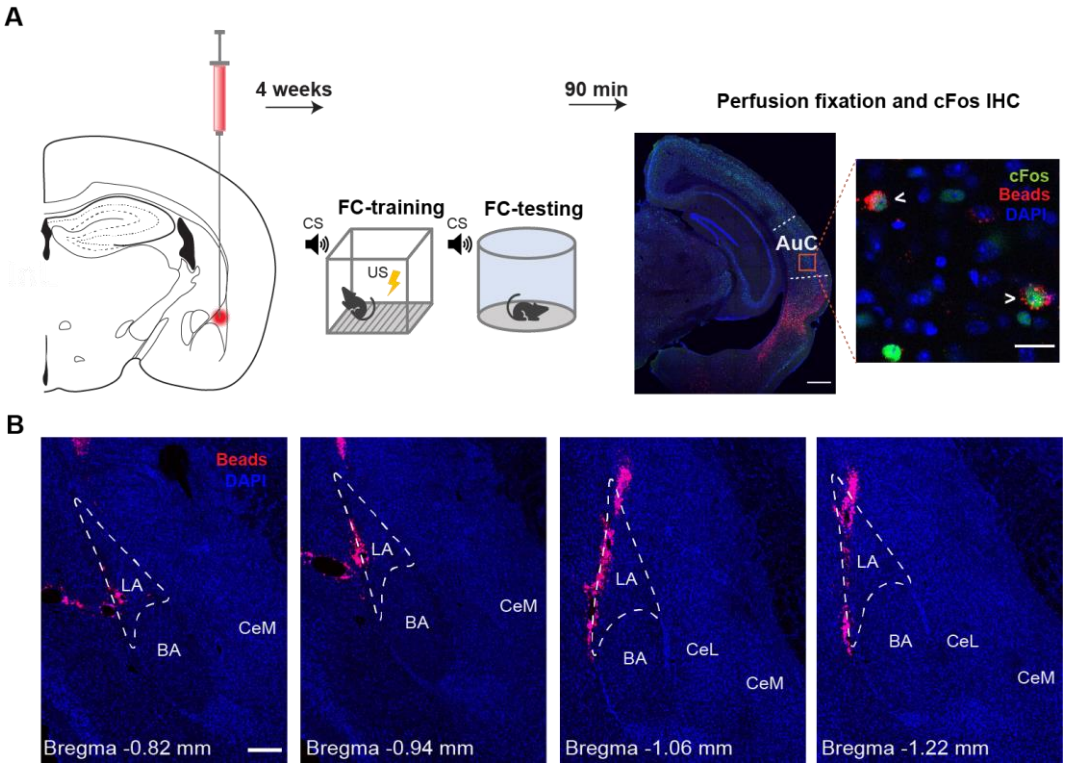

Figure 20: Retrograde tracing of projections to the LA. A) Experimental design. Retrobeads™ were stereotactically delivered into the LA. Afterwards, mice were housed in groups for 4 weeks before FC to enable the beads travelling up the axons and accumulating in the cell body of neurons that project to the LA. Mice were perfused transcardially 90 min after behavioral assessment. Left image: Low magnification overview of a brain slice containing the AC. Scale bar = 500 µm. Right image: High magnification photomicrograph of cells expressing cFos and RetroBeads™. Arrow heads mark double labeled cells. Scale bar = 20 µm. **B)** Sequence of brain slices obtained from one animal containing the RetroBeads™ injection site.

4 Discussion

The aim of this work was to shed a light on the mechanistic underpinnings of the pronounced deficit in auditory cued FC due observed in global Nlgn2 KO mice. Using a combination of behavioral assessment and cFos immunohistochemistry, we identified a deficit in neuronal activation within the LA of Nlgn2 KO mice, as well as coincident alterations in the activation pattern of VIP+ neurons. Even though this work primarily focused on the amygdala including its inhibitory circuits, our data strongly indicates that the deletion of Nlgn2 might result in a plasticity deficit in associative fear learning within upstream regions of the amygdala such as the mPFC or the AuC, both of which are critically implicated in learning and expression of conditioned fear responses (LeDoux 2000; Letzkus et al. 2011; Liang et al. 2015). Altogether, this work demonstrates that the lack of Nlgn2 severely perturbs the function of the brain wide fear processing network. The precise results and hypotheses on the origin of the deficit in FC observed in Nlgn2 KO mice are discussed in detail in the following section.

4.1 Consequences of Nlgn2 deletion on aversive behaviors

As described previously, Nlgn2 KO mice show a prominent anxiety phenotype (Blundell et al. 2009; Babaev et al. 2018a) in behavioral paradigms such as the OF investigating their innate aversion of exposed bright spaces. Consistent with these observations, we also found an anxiety-related increase in freezing behavior in our behavior data (Figure 6 B). On training day, naive Nlgn2 KO mice showed significantly increased freezing levels compared to their WT littermates when being placed in the conditioning chamber, representing a novel and potentially dangerous environment.

In sharp contrast, their ability to retrieve auditory cued fear memories was severely impaired (Figure 6 D). Nlgn2 KO mice that received paired FC training showed significantly less freezing behavior than conditioned WT mice after presentation of the CS on testing day. Importantly, H.A. tested motor and hearing ability of Nlgn2 KO mice by the acoustic startle response and the visual placement test and her unpublished data do not show any relevant impairments that could explain their phenotype in auditory cued FC, which is consistent with previous studies (Wöhr et al. 2013; Chen et al. 2019). Importantly, these findings confirm that innate anxiety and acquired fear are mediated by different neural circuits and entirely distinct molecular mechanisms. Interestingly, we further found that both Nlgn2 and WT control animals did not freeze at all on testing day (Figure 6 C-D), which might be due to a

habituation mechanism which was not further pursued in this study. Whether the deficit of Nlgn2 KO mice in FC mechanistically arises already during memory acquisition, during consolidation or during fear recall, as measured in our experiment, has not yet been elucidated, and only few studies addressed this specific question to date. For instance, it has been shown that virus-mediated conditional Nlgn2 (cNlgn2) KO within the mPFC partially reproduces the deficit in fear recall of cued fear memories observed in global Nlgn2 KO mice when the KO is conducted before FC training, but not when it is performed after FC training (Liang et al. 2015). These findings indicate that at least within the mPFC, the learning process might be impaired by Nlgn2 deletion, whereas the capability of fear recall appears to be unaffected. However, given that the FC paradigm conducted by Liang and colleagues differs from ours especially in terms of the waiting period between FC training and testing, one cannot directly refer these results to our experiments.

4.2 Consequences of Nlgn2 deletion on the amygdala fear circuitry

The notion of the amygdala being critically implicated in acquisition and expression of learned fear is widely accepted in the scientific world supported by a huge body of studies (Wolff et al. 2014; Janak und Tye 2015; Tovote et al. 2015). Below, I will discuss the findings of this study in the context of what is known so far about amygdala fear circuitries and the respective circuit mechanisms.

4.2.1 Effects of Nlgn2 deletion on neurons in the LA

In line with previous studies showing that plasticity within the LA after convergence of the CS and the US is required for associative fear learning (Rosenkranz und Grace 2002; Nabavi et al. 2014), we demonstrate that Nlgn2 KO mice have alterations in neuronal activation as assessed by cFos quantification (Figure 8 C). While WT mice show a strong increase in cFos expression after presentation of the CS when they received paired training beforehand, this effect cannot be observed in Nlgn2 KO mice. Further, there is a strong interaction of FC training and the genotype as revealed by two-way ANOVA. In direct comparison of mice of both genotypes that received paired training, WT mice only show a trend towards higher activation of the LA which is not significant. Here, the most likely explanation would be that the results include an overlapping anxiety-related increase of cFos expression in Nlgn2 KO mice.

Consistent with the observation that Nlgn2 KO mice show alterations in the activation pattern within the LA that are presumably related to FC, we also detected changes in local inhibitory interneurons. Surprisingly, the most robust effect was observed in VIP+ neurons, which appear to act contrarily in WT and Nlgn2 KO mice. In WT mice, VIP+ neurons were higher activated in control animals and slightly decreased their firing in trained animals, whereas in Nlgn2 KO mice they showed a strong increase in cFos expression in trained animals (Figure 9 F). Similar to what has been demonstrated for cortical regions (Pi et al. 2013; Letzkus et al. 2015), VIP+ neurons within the BLA were shown to primarily target other interneurons that form synapses onto pyramidal neurons and are therefore perfectly positioned to disinhibit projection neurons (Rhomberg et al. 2018; Krabbe et al. 2019). Further, VIP+ neurons are activated by the aversive US during fear conditioning and their enhanced firing during associative fear learning was shown being necessarily required for memory formation (Krabbe et al. 2019). Although our data strongly point towards an implication of VIP+ neurons in the Nlgn2 phenotype in FC, VIP+ neurons are a heterogenous group (Rhomberg et al. 2018), which makes hard to interpret our data at this level and to develop a precise model. However, the notion that Nlgn2 deletion perturbs the function of VIP+ neurons within the BLA is perfectly in line with previous literature attributing an important role to VIP+ neurons in associative fear learning. Altogether, VIP+ neurons are particularly interesting candidate for further experiments.

4.2.2 Effects of Nlgn2 deletion on neurons in the BA

In contrast to the LA, overall cFos quantification of the BA did not uncover a fear-related increase in neuronal activation neither in WT nor in Nlgn2 KO mice, but a generally increased number of cFos-expressing nuclei in Nlgn2 KO mice (Figure 8 D). This phenomenon is highly consistent with the previous finding that Nlgn2 KO mice show an anxiety-related overactivation of the BA when being exposed to the OF (Babaev et al. 2018a) and thus, nicely reproduces their anxiety phenotype on the cellular level, which is also showing up in the behavior data (Figure 6 B). In line with the observation that Nlgn2 KO mice show an overactivation of the BA that is presumably related to anxiety rather than conditioned fear expression, we did not detect significant changes in the activation pattern of BA inhibitory neurons. Unfortunately, the existing antibodies against calcium/calmodulin-dependent protein kinase II (CaMKII), a marker for glutamatergic neurons, are extremely unreliable, prohibiting to demonstrate that the detected changes in BA of Nlgn2 KO mice occur in excitatory neurons. However, considering that the BLA is a

cortical-like structure that mainly consists of glutamatergic neurons (Sah et al. 2003), one can assume that the activation pattern in these populations must be altered given that we detected differences in the general expression of neuronal activity marker cFos. In addition, this assumption is in line with the previous finding of our group that CaMKII+ neurons show higher activation under anxiogenic conditions, whereas the activation pattern of PV+ and SOM+ neurons remains unaffected (Babaev et al. 2016).

4.2.3 Effects of Nlgn2 deletion on amygdala downstream regions

Since we sought to find a downstream correlate for the deficit in FC caused by Nlgn2 deletion, I further assessed neuronal activation of the CeA as well as of the vlPAG performing cFos induction assay.

Astonishingly, given that the existing literature provides strong evidence that local microcircuits within the CeL formed by SOM+ and PKC-δ+ neurons play a pivotal role during different stages of FC paradigms (Haubensak et al. 2010; Gafford und Ressler 2016), neither overall cFos quantification (Figure 8 E) nor cell-specific cFos quantification (Figure 11 C, D) revealed significant effects in the CeL. Within the CeM, the main output nucleus of the amygdala, the general cFos analysis did not reveal any effects either (Figure 8 F), but there was a genotype-based effect in SOM+ neurons (Figure 11 E) that might in some extend contribute to the phenotype in FC, but which was not further pursued in this work. However, the fact that our data do not show manifest effects within the CeA could either be due to methodical issues, or it could be a genuine result showing that the CeA is not implicated in the Nlgn2 phenotype in FC. Especially for the CeL, our approach reached its limitations since there are a huge amount of SOM+ fibers making it exceedingly hard to clearly identify SOM+ cells during the quantification process (Figure 18 B). A possibility to overcome this issue in following experiments would be to first cross the SOM-Cre driver mice with the CAG-CAT-EGFP line to generate the mice I used for my validation experiment (Figure 17 B, D) and in a second step to cross them with regular Nlgn2 KO mice.

The vlPAG is a downstream target of amygdala projection neurons and presumably one of the main regions in mediating freezing behavior and other defensive behaviors in response to a threat (Tovote et al. 2016). Strikingly, there was no difference in cFos levels in WT and Nlgn2 KO mice, but there was a modest main effect of FC training ($p < 0.05$) (Figure 15 B). In this case, we cannot rule out that shifts in activation of local neurons in vlPAG were simply not detected by quantification of overall cFos expression, given that we did not dissect different cell types. PAG anatomy is complex: CeL SOM+ projection neurons presumably

target inhibitory populations in vlPAG (Oka et al. 2008; Penzo et al. 2015) which, in turn, form synapses onto local glutamatergic neurons (Tovote et al. 2016). Further, these projection neurons can be divided into smaller subpopulations that were shown being differentially activated during freezing, indicating that freezing, analgesia and flight as parts of the defensive reaction might be generated by distinct glutamatergic neuronal populations (Tovote et al. 2016). An alternative reason why changes in the activation pattern of Nlgn2 KO mice might not be detected, could be that cFos is not a suitable marker for neuronal activity within the vlPAG. Since little is known about the specific intracellular pathways that result into an upregulation of cFos expression in particular neurons within the brainstem, it is still possible that the measured cFos levels reflect something other than neural activity. To rule this out, it would be necessary to test other IEG markers such as the activity-regulated cytoskeleton-associated protein, Zif/268 and the neuronal PAS domain protein 4 and to subsequently conduct an induction assay to directly compare the quantification results.

4.3 Consequences of Nlgn2 deletion on the AuC

The implications of the AuC in associative learning related to sounds have been addressed in a wide range of studies. The emerging picture strongly indicates that AuC neurons can be engaged by both the tone and the aversive foot shock and that both signals converge onto AuC neurons (Letzkus et al. 2011; Letzkus et al. 2015). In addition, their temporal coincidence during FC learning was shown to induce plastic circuit modifications (Schreiner und Polley 2014). In accordance with previous literature, my data demonstrates that WT mice show an upregulation in cFos expression within the AuC, particularly in Au1, following the presentation of the CS on testing day when they received paired FC training beforehand. In stark contrast, the opposite is the case with Nlgn2 KO mice, which even show the reverse tendency and thus presumably exhibit a deficit in neuronal plasticity in the context of auditory cued FC (Figure 12 B). The observation that unconditioned Nlgn2 KO mice even have a tendency towards higher cFos expression than their WT littermates supports the assumption that their behavioral phenotype in FC cannot be explained by a deficit in hearing ability. Furthermore, hearing ability of Nlgn2 KO mice has been tested by our group prior to behavioral experiments and, in line with previous literature (Chen et al. 2019), no relevant effects that could explain their phenotype in FC were observed (unpublished data). Importantly, it has been demonstrated that chemogenetic inhibition of neurons within the AuC that are activated by the foot shock impairs the animals' capability to identify aversive sounds (Grosso et al. 2015). This finding demonstrates that the convergence of the CS and

the US within the AuC is compellingly required to recognize the valence of a tone and, consequently, to exhibit an adapted behavioral response (Concina et al. 2019). From this perspective, the detected cFos pattern including the deficit in expression in conditioned Nlgn2 KO mice makes perfect sense and could possibly provide an explanation for their impaired ability to retrieve auditory cued fear memories.

Similar to what has been shown for other brain areas of the neocortex (Lee et al. 2013; Pfeffer et al. 2013; Pi et al. 2013), the firing of pyramidal neurons within the AuC is tightly regulated by a local inhibitory network (Pi et al. 2013). A continuously growing number of studies provide evidence that foot shocks reach the AuC through cholinergic projections from the basal forebrain and that acetylcholine-receptor expressing VIP+ neurons can be engaged by aversive foot shocks (Letzkus et al. 2011; Pi et al. 2013; Fu et al. 2015). A widespread model on how local inhibitory neurons in the cortex facilitate learning processes includes the idea of disinhibition as a main circuit mechanism (Letzkus et al. 2015). Feedback information on the valence of the tone reaches VIP+ neurons which, in turn, provide inhibition on SOM+ and/or PV+ neurons and thereby disinhibit pyramidal neurons (Figure 13 D) (Pi et al. 2013; Letzkus et al. 2015). In addition, cFos expression of VIP+ neurons in AuC was shown to correlate with freezing behavior in auditory cued FC (Melzer et al. 2021). Based on this fundament of knowledge, we decided to conduct a cell-specific cFos analysis on interneurons in Au1 where the changes in Nlgn2 KO mice detected by overall cFos quantification were the most prominent. The finding of VIP+ neurons showing an increase in cFos expression in conditioned animals (Figure 13 A) is highly consistent with the literature and at least in WT animals, this activation pattern is in line with the disinhibition of neurons in Au1 revealed by general cFos quantification (Figure 12 B). Further, the trend towards higher activation of VIP+ neurons in conditioned WT mice compared to their Nlgn2 KO littermates (Figure 13 B) corresponds with the observed behavioral phenotype and with their lack of disinhibition within the Au1. Interestingly, we observed a reduction in the total number of detected VIP+ neurons in conditioned Nlgn2 KO mice (Figure 13 F), which could be due to a degradation of VIP in those neurons. However, it remains to be determined how PV+ and SOM+ neurons match this theory. With respect to this particular question, the literature indicates a prominent role of SOM+ neurons in cortical disinhibitory circuits (Pfeffer et al. 2013; Pi et al. 2013), which were only insufficiently studied in this work. Nevertheless, the emerging picture arising from this data supports a model in which the lack of Nlgn2 results in a plasticity deficit of VIP+ neurons leading to reduced disinhibition of pyramidal neurons within Au1 which could likely contribute to the Nlgn2 KO phenotype in FC. However,

despite the fact that this is currently the most likely hypothesis according to the data, it still needs to be validated and strengthened with further experiments.

4.4 Interaction of the LA and the AuC in auditory cued FC

Now that the individual results of both the LA and the AuC have been discussed above in detail, it remains to be determined if the observed effects of Nlgn2 deletion in both regions might be related to each other. Both the LA and the AuC, send out reciprocal projections to each other that induce long-lasting plastic circuit modifications, respectively (Romanski et al. 1993; Tsvetkov et al. 2002; Yang et al. 2016). Moreover, these pathways were shown being critically involved in the expression of learned fear (Tsvetkov et al. 2002; Boatman und Kim 2006). Using chemo- and optogenetics, it has been shown that silencing of a specific pathway from the LA to the AuC severely perturbs the expression of learned fear to auditory cues (Yang et al. 2016). On the other hand, a similar effect was observed in rats through specific silencing of terminals reaching the BLA from the AuC (Manassero et al. 2018). In this study, we found a decreased cFos expression indicating a plasticity deficit in Nlgn2 KO mice which was present in both regions, albeit being more pronounced in the AuC (Figure 8 C, Figure 12 B). Thus, in the context of previous literature, the question whether and to what extent these results are related to each other is a particularly interesting one which future work of our group will aim at providing an answer to.

4.5 Methodical chances and limitations

In this study, the main tool to measure neuronal activation was cFos quantification based on immunohistochemistry. Albeit being a well-established method, the cFos approach reaches its limits in terms of temporal resolution when investigating neuronal activation patterns that directly correlate with an observed behavior. Furthermore, this approach only allowed an assessment of changes that occur during fear retrieval, whereas it was impossible to investigate the effects during acquisition of the fear memory, assuming that neuronal firing induced by the foot shock would have obscured the relevant effects. On the other hand, cFos quantification facilitates an excellent quantitative estimation of neuronal activation, given that it allows to analyze many neurons at the same time. On the contrary, the alternative method, deep-brain calcium imaging, can only be applied to small number of neurons at a time. Even though calcium imaging has an excellent temporal resolution and hence, is a suitable method to characterize dynamic changes in neural circuits, it is extremely expensive

and requires extensive technical expertise. cFos immunohistochemistry is much less costly, but also a very time-consuming method. In conclusion, one can say that cFos quantification is a good method to conduct a screening of different brain regions and once a likely candidate has been identified, calcium imaging can provide more accurate information.

Further, immunohistochemistry becomes complex when it is used for quantitative assessment of subtle circuit effects such as we aimed to measure in this work. First, antigenicity of the brain tissue itself is critically dependent on several variables including the age of the tissue and its pH value. Second, the staining quality further depends on several factors like the antibodies staining properties and specificity as well as the concentration of the antigen. Last, image analysis is always dependent on the person who conducts the analysis and there is variance caused by the experimenter which can be reduced with widely automized quantification processes, but not entirely avoided. Altogether, these effects caused variance between sets of mice for which reason the data was finally normalized.

Another important aspect to keep in mind is that the neuropeptides which were used as simple neuronal markers to label distinct cell types also have physiological functions in neurons. Thus, we had to consider that their concentration might be up- or downregulated either in response to FC or as consequence of a genotype-based effect resulting in a reduced number of cells detected by the antibody. To rule out the results might be biased due to that reason, the number of detected cells per animal and region was quantified either.

4.6 Outlook

Altogether, the data presented in this work provide a broad basis for further experiments, some of which have already been outlined in previous sections. Despite the fact that we were able to detect changes in various fear-associated brain regions in Nlgn2 KO mice, different pieces of information obtained by various experimental approaches are still required to provide a complete picture of the mechanistic consequences of Nlgn2 deletion on associative fear learning.

Certainly, the first step will be to define which of the investigated brain areas is the primary source of the alterations in the activation pattern observed in Nlgn2, which is likely due to a deficit in synaptic plasticity. For this purpose, it will be essential to perform local virus-mediated Nlgn2 deletions through stereotactic microinjections and to figure out whether the effects sufficiently reproduce the phenotype of global Nlgn2 KO mice in FC. Once this step has been taken, a whole series of new questions arises. First, what happens during FC training

within this particular region? So far, our work based on cFos immunohistochemistry exclusively focused on effects that occur after fear recall, but we were not able to address the circuit the mechanisms that occur during fear acquisition. Given that cFos is a virtually unspecific marker for neuronal activation, we suspected that the neuronal representation of the foot shock would mask the actual effects of fear learning that we meant to specify. A suitable way to overcome this issue would be to perform deep-brain calcium imaging of specific neuronal populations during fear learning which additionally allows a distinction between different cell types.

Another important question yet unanswered is how the different brain regions interact with each other in cued FC. The fear-processing network consists of various brain areas some of which showed altered activation patterns in Nlgn2 KO mice. A combination of retro- and anterograde circuit tracing with either local RetroBeads™ or virus injections and cFos immunohistochemistry would allow to investigate the activation patterns of specific projections between brain regions and, hence, permit a conclusion on how the distinct findings might be related to each other.

Since our data indicate a possible effect of VIP+ neurons, special attention should be paid to this subpopulation. Again, calcium imaging would be an appropriate approach to address this issue. Further, it would be interesting to see whether an interneuron specific Nlgn2 KO reproduces the phenotype in FC. This experiment would require a crossing of the Cre driver animals I validated (Figure 17) with cNlgn2 KO animals. Last, it would be important to demonstrate that Nlgn2 is expressed in synapses onto VIP+ neurons within the particular brain region of interest, what could be realized through synaptic staining of VIP-Cre driver mice.

5 Conclusion

In the past decades, strong evidence arose that the emergence of a large variety of neuropsychiatric conditions is caused by perturbations of the synaptic transmission on the molecular level. The synapse is the key structure of neural networks since it enables neurons to communicate with others and to precisely coordinate their firing to generate a specific behavioral output. Due to its pivotal role in GABAergic transmission, the inhibitory synapse organizer Neuroligin-2 is a particularly interesting candidate potentially contributing to the emergence of neuropsychiatric conditions. In accordance with this notion, various mutations in NLGN2 gene have been associated with neuropsychiatric disorders such as autism spectrum disorder, schizophrenia and anxiety disorders.

Transgenic mouse lines provide a valuable tool to study how perturbed Neuroligin-2 function is translated into deviant behavior. In this study, we sought to elucidate the circuit mechanisms underlying the impaired ability of global Neuroligin-2 knockout mice to retrieve fear memories in auditory cued fear conditioning, a well-established behavioral paradigm to investigate associative fear learning. To address this question, a combination of behavioral assessment and cFos immunohistochemistry was applied. Pursuing a top-bottom approach, we first identified changes in the activation pattern of several fear-related brain regions in Neuroligin-2 knockout mice. In particular, Neuroligin-2 knockout mice show altered activation patterns in the lateral amygdala and the auditory cortex, both of which were previously shown underlying plastic circuit rearrangements induced by temporal coincidence of the foot shock and the tone. Further, VIP-expressing neurons in both regions showed an aberrant activation pattern, indicating that their function might be altered by Neuroligin-2 deletion and making them a likely candidate to potentially contribute to the Neuroligin-2 phenotype in fear conditioning.

Together, my findings shed a first light on the mechanistic underpinnings of the Neuroligin-2 knockout phenotype in fear conditioning, but also highlight the complexity of the implications of Neuroligin-2 in the fear circuit. Further, this work constitutes a fundament for subsequent experiments including local virus mediated Neuroligin-2 deletions as well as in vivo approaches such as deep-brain calcium imaging. In the long term, further research based on this work may succeed to identify potential targets for more specific drug treatment of fear-related disorders.

6 References

Alber M, Kalscheuer VM, Marco E, Sherr E, Lesca G, Till M, Gradek G, Wiesener A, Korenke C, Mercier S, et al. (2017): *ARHGEF9* disease: Phenotype clarification and genotype-phenotype correlation. Neurol Genet 3, e148

Ali H, Marth L, Krueger-Burg D (2020): Neuroligin-2 as a central organizer of inhibitory synapses in health and disease. Sci Signal 13, eabd8379

Amano T, Duvarci S, Popa D, Paré D (2011): The fear circuit revisited: contributions of the basal amygdala nuclei to conditioned fear. J Neurosci 31, 15481–15489

Andero R, Dias BG, Ressler KJ (2014): A role for Tac2, NkB, and Nk3 receptor in normal and dysregulated fear memory consolidation. Neuron 83, 444–454

Armony JL, Quirk GJ, LeDoux JE (1998): Differential effects of amygdala lesions on early and late plastic components of auditory cortex spike trains during fear conditioning. J Neurosci 18, 2592–2601

Aschauer D, Rumpel S (2018): The Sensory Neocortex and Associative Memory. Curr Top Behav Neurosci 37, 177–211

Babaev O, Botta P, Meyer E, Müller C, Ehrenreich H, Brose N, Lüthi A, Krueger-Burg D (2016): Neuroligin 2 deletion alters inhibitory synapse function and anxiety-associated neuronal activation in the amygdala. Neuropharmacology 100, 56–65

Babaev O, Cruces-Solis H, Piletti Chatain C, Hammer M, Wenger S, Ali H, Karalis N, de Hoz L, Schlüter OM, Yanagawa Y, et al. (2018a): IgSF9b regulates anxiety behaviors through effects on centromedial amygdala inhibitory synapses. Nat Commun 9, 5400

Babaev O, Piletti Chatain C, Krueger-Burg D (2018b): Inhibition in the amygdala anxiety circuitry. Exp Mol Med 50, 18

Bemben MA, Shipman SL, Nicoll RA, Roche KW (2015): The cellular and molecular landscape of neuroligins. Trends Neurosci 38, 496–505

Binda CS, Nakamura Y, Henley JM, Wilkinson KA (2019): Sorting nexin 27 rescues neuroligin 2 from lysosomal degradation to control inhibitory synapse number. Biochem J 476, 293–306

Blundell J, Tabuchi K, Bolliger MF, Blaiss CA, Brose N, Liu X, Südhof TC, Powell CM (2009): Increased anxiety-like behavior in mice lacking the inhibitory synapse cell adhesion molecule neuroligin 2. Genes Brain Behav 8, 114–126

Boatman JA, Kim JJ (2006): A thalamo-cortico-amygdala pathway mediates auditory fear conditioning in the intact brain. Eur J Neurosci 24, 894–900

Brady KT, Killeen TK, Brewerton T, Lucerini S (2000): Comorbidity of psychiatric disorders and posttraumatic stress disorder. J Clin Psychiatry 61, 22–32

Buzsáki G, Wang XJ (2012): Mechanisms of gamma oscillations. Annu Rev Neurosci 35, 203–225

Capogna M (2014): GABAergic cell type diversity in the basolateral amygdala. Curr Opin Neurobiol 26, 110–116

Chaudhuri A, Zangenehpour S, Rahbar-Dehgan F, Ye F (2000): Molecular maps of neural activity and quiescence. Acta Neurobiol Exp (Warsz) 60, 403–410

Chen C, Krueger-Burg D, de Hoz L (2019): Wide sensory filters underlie performance in memory-based discrimination and generalization. PloS One 14, e0214817

Chen P, Lou S, Huang ZH, Wang Z, Shan QH, Wang Y, Yang Y, Li X, Gong H, Jin Y, et al. (2020): Prefrontal Cortex Corticotropin-Releasing Factor Neurons Control Behavioral Style Selection under Challenging Situations. Neuron 106, 301–315

Chih B, Engelman H, Scheiffele P (2005): Control of excitatory and inhibitory synapse formation by neuroligins. Science 307, 1324–1328

Ciocchi S, Herry C, Grenier F, Wolff SBE, Letzkus JJ, Vlachos I, Ehrlich I, Sprengel R, Deisseroth K, Stadler MB, et al. (2010): Encoding of conditioned fear in central amygdala inhibitory circuits. Nature 468, 277–282

Concina G, Renna A, Grosso A, Sacchetti B (2019): The auditory cortex and the emotional valence of sounds. Neurosci Biobehav Rev 98, 256–264

Corcoran KA, Quirk GJ (2007): Activity in prelimbic cortex is necessary for the expression of learned, but not innate, fears. J Neurosci 27, 840–844

Courtin J, Bienvenu TCM, Einarsson EÖ, Herry C (2013): Medial prefrontal cortex neuronal circuits in fear behavior. Neuroscience 240, 219–242

Craske MG, Stein MB (2016): Anxiety. Lancet 388, 3048–3059

Curtis D (2016): Practical Experience of the Application of a Weighted Burden Test to Whole Exome Sequence Data for Obesity and Schizophrenia. Ann Hum Genet 80, 38–49

Dejanovic B, Lal D, Catarino CB, Arjune S, Belaidi AA, Trucks H, Vollmar C, Surges R, Kunz WS, Motameny S, et al. (2014): Exonic microdeletions of the gephyrin gene impair GABAergic synaptic inhibition in patients with idiopathic generalized epilepsy. Neurobiol Dis 67, 88–96

Ehrlich I, Humeau Y, Grenier F, Ciocchi S, Herry C, Lüthi A (2009): Amygdala inhibitory circuits and the control of fear memory. Neuron 62, 757–771

Fadok JP, Krabbe S, Markovic M, Courtin J, Xu C, Massi L, Botta P, Bylund K, Müller C, Kovacevic A, et al. (2017): A competitive inhibitory circuit for selection of active and passive fear responses. Nature 542, 96–100

Fanselow MS, Poulos AM (2005): The neuroscience of mammalian associative learning. Annu Rev Psychol 56, 207–234

Fu Y, Kaneko M, Tang Y, Alvarez-Buylla A, Stryker MP (2015): A cortical disinhibitory circuit for enhancing adult plasticity. Elife 4, e05558

Gafford GM, Ressler KJ (2016): Mouse models of fear-related disorders: Cell-type-specific manipulations in amygdala. Neuroscience 321, 108–120

Gilpin NW, Herman MA, Roberto M (2015): The central amygdala as an integrative hub for anxiety and alcohol use disorders. Biol Psychiatry 77, 859–869

Graf ER, Zhang X, Jin SX, Linhoff MW, Craig AM (2004): Neurexins induce differentiation of GABA and glutamate postsynaptic specializations via neuroligins. Cell 119, 1013–1026

Grewe BF, Gründemann J, Kitch LJ, Lecoq JA, Parker JG, Marshall JD, Larkin MC, Jercog PE, Grenier F, Li JZ, et al. (2017): Neural ensemble dynamics underlying a long-term associative memory. Nature 543, 670–675

Grosso A, Cambiaghi M, Concina G, Sacco T, Sacchetti B (2015): Auditory cortex involvement in emotional learning and memory. Neuroscience 299, 45–55

Gu Y, Piper WT, Branigan LA, Vazey EM, Aston-Jones G, Lin L, LeDoux JE, Sears RM (2020): A brainstem-central amygdala circuit underlies defensive responses to learned threats. Mol Psychiatry 25, 640–654

Haubensak W, Kunwar PS, Cai H, Ciocchi S, Wall NR, Ponnusamy R, Biag J, Dong HW, Deisseroth K, Callaway EM, et al. (2010): Genetic dissection of an amygdala microcircuit that gates conditioned fear. Nature 468, 270–276

Hayashi-Takagi A (2017): Synapse pathology and translational applications for schizophrenia. Neurosci Res 114, 3–8

Heshmati M, Aleyasin H, Menard C, Christoffel DJ, Flanigan ME, Pfau ML, Hodes GE, Lepack AE, Bicks LK, Takahashi A, et al. (2018): Cell-type-specific role for nucleus accumbens neuroligin-2 in depression and stress susceptibility. Proc Natl Acad Sci U S A 115, 1111–1116

Hines RM, Wu L, Hines DJ, Steenland H, Mansour S, Dahlhaus R, Singaraja RR, Cao X, Sammler E, Hormuzdi SG, et al. (2008): Synaptic imbalance, stereotypies, and impaired social interactions in mice with altered neuroligin 2 expression. J Neurosci 28, 6055–6067

Hippenmeyer S, Vrieseling E, Sigrist M, Portmann T, Laengle C, Ladle DR, Arber S (2005): A developmental switch in the response of DRG neurons to ETS transcription factor signaling. PLoS Biol 3, e159

Hunt S, Sun Y, Kucukdereli H, Klein R, Sah P (2017): Intrinsic Circuits in the Lateral Central Amygdala. eNeuro 4, 0367–16.2017

Ichtchenko K, Nguyen T, Südhof TC (1996): Structures, alternative splicing, and neurexin binding of multiple neuroligins. J Biol Chem 271, 2676–2682

Janak PH, Tye KM (2015): From circuits to behaviour in the amygdala. Nature 517, 284–292

Jedlicka P, Hoon M, Papadopoulos T, Vlachos A, Winkels R, Poulopoulos A, Betz H, Deller T, Brose N, Varoqueaux F, Schwarzacher SW (2011): Increased dentate gyrus excitability in neuroligin-2-deficient mice in vivo. Cereb Cortex 21, 357–367

Johansen JP, Tarpley JW, LeDoux JE, Blair HT (2010): Neural substrates for expectation-modulated fear learning in the amygdala and periaqueductal gray. Nat Neurosci 13, 979–986

Kasem E, Kurihara T, Tabuchi K (2018): Neurexins and neuropsychiatric disorders. Neurosci Res 127, 53–60

Kathuria A, Lopez-Lengowski K, Watmuff B, McPhie D, Cohen BM, Karmacharya R (2019): Synaptic deficits in iPSC-derived cortical interneurons in schizophrenia are mediated by NLGN2 and rescued by N-acetylcysteine. Transl Psychiatry 9, 321

Kemppainen S, Pitkänen A (2000): Distribution of parvalbumin, calretinin, and calbindin-D(28k) immunoreactivity in the rat amygdaloid complex and colocalization with gamma-aminobutyric acid. J Comp Neurol 426, 441–467

Kim J, Zhang X, Muralidhar S, LeBlanc SA, Tonegawa S (2017): Basolateral to central amygdala neural circuits for appetitive behaviors. Neuron 93, 1464-1479.e5

Kleijer KTE, Schmeisser MJ, Krueger DD, Boeckers TM, Scheiffele P, Bourgeron T, Brose N, Burbach JPH (2014): Neurobiology of autism gene products: towards pathogenesis and drug targets. Psychopharmacology (Berl) 231, 1037–1062

Koehnke J, Jin X, Budreck EC, Posy S, Scheiffele P, Honig B, Shapiro L (2008): Crystal structure of the extracellular cholinesterase-like domain from neuroligin-2. Proc Natl Acad Sci U S A 105, 1873–1878

Koide T, Banno M, Aleksic B, Yamashita S, Kikuchi T, Kohmura K, Adachi Y, Kawano N, Kushima I, Nakamura Y, et al. (2012): Common variants in MAGI2 gene are associated with increased risk for cognitive impairment in schizophrenic patients. PloS One 7, e36836

Krabbe S, Paradiso E, d'Aquin S, Bitterman Y, Courtin J, Xu C, Yonehara K, Markovic M, Müller C, Eichlisberger T, et al. (2019): Adaptive disinhibitory gating by VIP interneurons permits associative learning. Nat Neurosci 22, 1834–1843

Krueger DD, Tuffy LP, Papadopoulos T, Brose N (2012): The role of neurexins and neuroligins in the formation, maturation, and function of vertebrate synapses. Curr Opin Neurobiol 22, 412–422

Krueger-Burg D, Papadopoulos T, Brose N (2017): Organizers of inhibitory synapses come of age. Curr Opin Neurobiol 45, 66–77

Laurent V, Westbrook RF (2009): Inactivation of the infralimbic but not the prelimbic cortex impairs consolidation and retrieval of fear extinction. Learn Mem 16, 520–529

LeDoux JE (2000): Emotion circuits in the brain. Annu Rev Neurosci 23, 155–184

LeDoux JE, Iwata J, Cicchetti P, Reis DJ (1988): Different projections of the central amygdaloid nucleus mediate autonomic and behavioral correlates of conditioned fear. J Neurosci 8, 2517–2529

Lee S, Kruglikov I, Huang ZJ, Fishell G, Rudy B (2013): A disinhibitory circuit mediates motor integration in the somatosensory cortex. Nat Neurosci 16, 1662–1670

Letzkus JJ, Wolff SBE, Meyer EMM, Tovote P, Courtin J, Herry C, Lüthi A (2011): A disinhibitory microcircuit for associative fear learning in the auditory cortex. Nature 480, 331–335

Letzkus JJ, Wolff SBE, Lüthi A (2015): Disinhibition, a Circuit Mechanism for Associative Learning and Memory. Neuron 88, 264–276

Li H, Penzo MA, Taniguchi H, Kopec CD, Huang ZJ, Li B (2013): Experience-dependent modification of a central amygdala fear circuit. Nat Neurosci 16, 332–339

Liang J, Xu W, Hsu Y-T, Yee AX, Chen L, Südhof TC (2015): Conditional neuroligin-2 knockout in adult medial prefrontal cortex links chronic changes in synaptic inhibition to cognitive impairments. Mol Psychiatry 20, 850–859

Lionel AC, Vaags AK, Sato D, Gazzellone MJ, Mitchell EB, Chen HY, Costain G, Walker S, Egger G, Thiruvahindrapuram B, et al. (2013): Rare exonic deletions implicate the synaptic organizer Gephyrin (GPHN) in risk for autism, schizophrenia and seizures. Hum Mol Genet 22, 2055–2066

Manassero E, Renna A, Milano L, Sacchetti B (2018): Lateral and Basal Amygdala Account for Opposite Behavioral Responses during the Long-Term Expression of Fearful Memories. Sci Rep 8, 518

Marro SG, Chanda S, Yang N, Janas JA, Valperga G, Trotter J, Zhou B, Merrill S, Yousif I, Shelby H, et al. (2019): Neuroligin-4 Regulates Excitatory Synaptic Transmission in Human Neurons. Neuron 103, 617-626.e6

Mascagni F, Muly EC, Rainnie DG, McDonald AJ (2009): Immunohistochemical characterization of parvalbumin-containing interneurons in the monkey basolateral amygdala. Neuroscience 158, 1541–1550

Mazuski C, Chen SP, Herzog ED (2020): Different Roles for VIP Neurons in the Neonatal and Adult Suprachiasmatic Nucleus. J Biol Rhythms 35, 465–475

McDonald AJ (1985): Immunohistochemical identification of gamma-aminobutyric acid-containing neurons in the rat basolateral amygdala. Neurosci Lett 53, 203–207

McDonald AJ (1987): Organization of amygdaloid projections to the mediodorsal thalamus and prefrontal cortex: a fluorescence retrograde transport study in the rat. J Comp Neurol 262, 46–58

Melzer S, Newmark ER, Mizuno GO, Hyun M, Philson AC, Quiroli E, Righetti B, Gregory MR, Huang KW, Levasseur J, et al. (2021): Bombesin-like peptide recruits disinhibitory cortical circuits and enhances fear memories. Cell 184, 5622-5634.e25

Morgan JI, Curran T (1988): Calcium as a modulator of the immediate-early gene cascade in neurons. Cell Calcium 9, 303–311

Muller JF, Mascagni F, McDonald AJ (2005): Coupled networks of parvalbumin-immunoreactive interneurons in the rat basolateral amygdala. J Neurosci 25, 7366–7376

Muller JF, Mascagni F, McDonald AJ (2007): Postsynaptic targets of somatostatin-containing interneurons in the rat basolateral amygdala. J Comp Neurol 500, 513–529

Nabavi S, Fox R, Proulx CD, Lin JY, Tsien RY, Malinow R (2014): Engineering a memory with LTD and LTP. Nature 511, 348–352

Nakamura T, Colbert MC, Robbins J (2006): Neural crest cells retain multipotential characteristics in the developing valves and label the cardiac conduction system. Circ Res 98, 1547–1554

Newport DJ, Nemeroff CB (2000): Neurobiology of posttraumatic stress disorder. Curr Opin Neurobiol 10, 211–218

Nguyen Q-A, Horn ME, Nicoll RA (2016): Distinct roles for extracellular and intracellular domains in neuroligin function at inhibitory synapses. Elife 5, e19236

Nguyen TA, Lehr AW, Roche KW (2020): Neuroligins and Neurodevelopmental Disorders: X-Linked Genetics. Front Synaptic Neurosci 12, 33

Numan M, Numan MJ (1994): Expression of Fos-like immunoreactivity in the preoptic area of maternally behaving virgin and postpartum rats. Behav Neurosci 108, 379–394

Oka T, Tsumori T, Yokota S, Yasui Y (2008): Neuroanatomical and neurochemical organization of projections from the central amygdaloid nucleus to the nucleus retroambiguus via the periaqueductal gray in the rat. Neurosci Res 62, 286–298

Pan-Vazquez A, Wefelmeyer W, Gonzalez Sabater V, Neves G, Burrone J (2020): Activity-Dependent Plasticity of Axo-axonic Synapses at the Axon Initial Segment. Neuron 106, 265–276

Papadopoulos T, Soykan T (2011): The role of collybistin in gephyrin clustering at inhibitory synapses: facts and open questions. Front Cell Neurosci 5, 11

Parente DJ, Garriga C, Baskin B, Douglas G, Cho MT, Araujo GC, Shinawi M (2017): Neuroligin 2 nonsense variant associated with anxiety, autism, intellectual disability, hyperphagia, and obesity. Am J Med Genet A 173, 213–216

Paxinos G, Franklin KBJ: The mouse brain in stereotaxic coordinates. 2nd ed; Academic Press, San Diego 2001

Penzo MA, Robert V, Li B (2014): Fear conditioning potentiates synaptic transmission onto long-range projection neurons in the lateral subdivision of central amygdala. J Neurosci 34, 2432–2437

Penzo MA, Robert V, Tucciarone J, De Bundel D, Wang M, Van Aelst L, Darvas M, Parada LF, Palmiter RD, He M, et al. (2015): The paraventricular thalamus controls a central amygdala fear circuit. Nature 519, 455–459

Peter M, Scheuch H, Burkard TR, Tinter J, Wernle T, Rumpel S (2012): Induction of immediate early genes in the mouse auditory cortex after auditory cued fear conditioning to complex sounds. Genes Brain Behav 11, 314–324

Pfeffer CK, Xue M, He M, Huang ZJ, Scanziani M (2013): Inhibition of inhibition in visual cortex: the logic of connections between molecularly distinct interneurons. Nat Neurosci 16, 1068–1076

Pi H-J, Hangya B, Kvitsiani D, Sanders JI, Huang ZJ, Kepecs A (2013): Cortical interneurons that specialize in disinhibitory control. Nature 503, 521–524

Pitman RK, Rasmusson AM, Koenen KC, Shin LM, Orr SP, Gilbertson MW, Milad MR, Liberzon I (2012): Biological studies of post-traumatic stress disorder. Nat Rev Neurosci 13, 769–787

Poulopoulos A, Aramuni G, Meyer G, Soykan T, Hoon M, Papadopoulos T, Zhang M, Paarmann I, Fuchs C, Harvey K, et al. (2009): Neuroligin 2 drives postsynaptic assembly at perisomatic inhibitory synapses through gephyrin and collybistin. Neuron 63, 628–642

Quirk GJ, Armony JL, LeDoux JE (1997): Fear Conditioning Enhances Different Temporal Components of Tone-Evoked Spike Trains in Auditory Cortex and Lateral Amygdala. Neuron 19, 613–624

Rainnie DG, Mania I, Mascagni F, McDonald AJ (2006): Physiological and morphological characterization of parvalbumin-containing interneurons of the rat basolateral amygdala. J Comp Neurol 498, 142–161

Rhomberg T, Rovira-Esteban L, Vikór A, Paradiso E, Kremser C, Nagy-Pál P, Papp OI, Tasan R, Erdélyi F, Szabó G, et al. (2018): Vasoactive Intestinal Polypeptide-Immunoreactive Interneurons within Circuits of the Mouse Basolateral Amygdala. J Neurosci 38, 6983–7003

Rogan MT, Stäubli UV, LeDoux JE (1997): Fear conditioning induces associative long-term potentiation in the amygdala. Nature 390, 604–607

Romanski LM, Clugnet MC, Bordi F, LeDoux JE (1993): Somatosensory and auditory convergence in the lateral nucleus of the amygdala. Behav Neurosci 107, 444–450

Rosenkranz JA, Grace AA (2002): Dopamine-mediated modulation of odour-evoked amygdala potentials during pavlovian conditioning. Nature 417, 282–287

Sagar SM, Sharp FR, Curran T (1988): Expression of c-fos protein in brain: metabolic mapping at the cellular level. Science 240, 1328–1331

Sah P, Faber ESL, Lopez De Armentia M, Power J (2003): The amygdaloid complex: anatomy and physiology. Physiol Rev 83, 803–834

Schizophrenia Working Group of the Psychiatric Genomics Consortium (2014): Biological insights from 108 schizophrenia-associated genetic loci. Nature 511, 421–427

Schreiner CE, Polley DB (2014): Auditory map plasticity: diversity in causes and consequences. Curr Opin Neurobiol 24, 143–156

Senn V, Wolff SBE, Herry C, Grenier F, Ehrlich I, Gründemann J, Fadok JP, Müller C, Letzkus JJ, Lüthi A (2014): Long-range connectivity defines behavioral specificity of amygdala neurons. Neuron 81, 428–437

Shyn SI, Shi J, Kraft JB, Potash JB, Knowles JA, Weissman MM, Garriock HA, Yokoyama JS, McGrath PJ, Peters EJ, et al. (2011): Novel loci for major depression identified by genome-wide association study of Sequenced Treatment Alternatives to Relieve Depression and meta-analysis of three studies. Mol Psychiatry 16, 202–215

Sierra-Mercado D, Padilla-Coreano N, Quirk GJ (2011): Dissociable roles of prelimbic and infralimbic cortices, ventral hippocampus, and basolateral amygdala in the expression and extinction of conditioned fear. Neuropsychopharmacology 36, 529–538

Sloviter RS, Nilaver G (1987): Immunocytochemical localization of GABA-, cholecystokinin-, vasoactive intestinal polypeptide-, and somatostatin-like immunoreactivity in the area dentata and hippocampus of the rat. J Comp Neurol 256, 42–60

Soykan T, Schneeberger D, Tria G, Buechner C, Bader N, Svergun D, Tessmer I, Poulopoulos A, Papadopoulos T, Varoqueaux F, et al. (2014): A conformational switch in collybistin determines the differentiation of inhibitory postsynapses. EMBO J 33, 2113–2133

Spampanato J, Polepalli J, Sah P (2011): Interneurons in the basolateral amygdala. Neuropharmacology 60, 765–773

Sumita K, Sato Y, Iida J, Kawata A, Hamano M, Hirabayashi S, Ohno K, Peles E, Hata Y (2007): Synaptic scaffolding molecule (S-SCAM) membrane-associated guanylate kinase with inverted organization (MAGI)-2 is associated with cell adhesion molecules at inhibitory synapses in rat hippocampal neurons. J Neurochem 100, 154–166

Sun C, Cheng MC, Qin R, Liao DL, Chen TT, Koong F-J, Chen G, Chen CH (2011): Identification and functional characterization of rare mutations of the neuroligin-2 gene (NLGN2) associated with schizophrenia. Hum Mol Genet 20, 3042–3051

Swanson LW (1981): A direct projection from Ammon's horn to prefrontal cortex in the rat. Brain Res 217, 150–154

Taniguchi H, He M, Wu P, Kim S, Paik R, Sugino K, Kvitsiani D, Kvitsani D, Fu Y, Lu J, et al. (2011): A resource of Cre driver lines for genetic targeting of GABAergic neurons in cerebral cortex. Neuron 71, 995–1013

Tovote P, Fadok JP, Lüthi A (2015): Neuronal circuits for fear and anxiety. Nat Rev Neurosci 16, 317–331

Tovote P, Esposito MS, Botta P, Chaudun F, Fadok JP, Markovic M, Wolff SBE, Ramakrishnan C, Fenno L, Deisseroth K, et al. (2016): Midbrain circuits for defensive behaviour. Nature 534, 206–212

Tsvetkov E, Carlezon WA, Benes FM, Kandel ER, Bolshakov VY (2002): Fear conditioning occludes LTP-induced presynaptic enhancement of synaptic transmission in the cortical pathway to the lateral amygdala. Neuron 34, 289–300

Uylings HB, van Eden CG (1990): Qualitative and quantitative comparison of the prefrontal cortex in rat and in primates, including humans. Prog Brain Res 85, 31–62

Varoqueaux F, Jamain S, Brose N (2004): Neuroligin 2 is exclusively localized to inhibitory synapses. Eur J Cell Biol 83, 449–456

Varoqueaux F, Aramuni G, Rawson RL, Mohrmann R, Missler M, Gottmann K, Zhang W, Südhof TC, Brose N (2006): Neuroligins determine synapse maturation and function. Neuron 51, 741–754

Vianna DM, Graeff FG, Brandão ML, Landeira-Fernandez J (2001): Defensive freezing evoked by electrical stimulation of the periaqueductal gray: comparison between dorsolateral and ventrolateral regions. Neuroreport 12, 4109–4112

Waite A, Brown SC, Blake DJ (2012): The dystrophin-glycoprotein complex in brain development and disease. Trends Neurosci 35, 487–496

Wang R, Dong JX, Wang L, Dong XY, Anenberg E, Jiang PF, Zeng LH, Xie YC (2019): A negative regulator of synaptic development: MDGA and its links to neurodevelopmental disorders. World J Pediatr 15, 415–421

Wang X, Kery R, Xiong Q (2018): Synaptopathology in autism spectrum disorders: Complex effects of synaptic genes on neural circuits. Prog Neuropsychopharmacol Biol Psychiatry 84, 398–415

Wöhr M, Silverman JL, Scattoni ML, Turner SM, Harris MJ, Saxena R, Crawley JN (2013): Developmental delays and reduced pup ultrasonic vocalizations but normal sociability in mice lacking the postsynaptic cell adhesion protein neuroligin2. Behav Brain Res 251, 50–64

Wolff SBE, Gründemann J, Tovote P, Krabbe S, Jacobson GA, Müller C, Herry C, Ehrlich I, Friedrich RW, Letzkus JJ, Lüthi A (2014): Amygdala interneuron subtypes control fear learning through disinhibition. Nature 509, 453–458

Xu W, Südhof TC (2013): A Neural Circuit for Memory Specificity and Generalization. Science 339, 1290–1295

Yang Y, Liu DQ, Huang W, Deng J, Sun Y, Zuo Y, Poo MM (2016): Selective synaptic remodeling of amygdalocortical connections associated with fear memory. Nat Neurosci 19, 1348–1355

Ye X, Kapeller-Libermann D, Travaglia A, Inda MC, Alberini CM (2017): Direct dorsal hippocampal-prelimbic cortex connections strengthen fear memories. Nat Neurosci 20, 52–61

Zhang B, Gokce O, Hale WD, Brose N, Südhof TC (2018): Autism-associated neuroligin-4 mutation selectively impairs glycinergic synaptic transmission in mouse brainstem synapses. J Exp Med 215, 1543–1553

Acknowledgements

First, I would like to express my gratitude to Prof. Dilja Krueger-Burg, my doctoral supervisor. She always put enormous trust in me, and I am deeply grateful for her support and her persistent guidance through my thesis.

Further, I would like to express my special thanks to Heba Ali, my direct supervisor in the lab. I have greatly benefited from her and from the contribution she made to this work.

I would also like to thank Prof. Thomas Bayer who, as a member of my thesis committee, gave insightful comments and suggestions on my project.

I appreciate the constructive comments and the valuable feedback on the manuscript offered by Marie Heber and Jonatan Hoffmann.

My special thanks go to the department of Hannelore Ehrenreich for generously providing their behavioral setup for our experimental purposes.

Last, I would like to thank the Brose department for making my work in lab so comfortable.